Copy
RM L51D30

NACA RM L51D30

45181

TECH LIBRARY KAFB, NM
0143854

NACA

RESEARCH MEMORANDUM

AN INVESTIGATION OF FLOW CHARACTERISTICS AT MACH NUMBER 4.04 OVER 6- AND 9-PERCENT-THICK SYMMETRICAL CIRCULAR-ARC AIRFOILS HAVING 30-PERCENT-CHORD TRAILING-EDGE FLAPS

By Edward F. Ulmann and Douglas R. Lord

Langley Aeronautical Laboratory
Langley Field, Va.

NATIONAL ADVISORY COMMITTEE
FOR AERONAUTICS

WASHINGTON
July 19, 1951

Classification cancelled (or changed to Unclassified)

By Authority of NASA Tech. Pub. Announcement #14

(OFFICER AUTHORIZED TO CHANGE)

By 22 Apr 67

NK

(GRADE OF OFFICER MAKING CHANGE)

3 Apr 61

DATE

TECH LIBRARY KAFB, NM
0143854

[redacted]

NATIONAL ADVISORY COMMITTEE FOR AERONAUTICS

RESEARCH MEMORANDUM

AN INVESTIGATION OF FLOW CHARACTERISTICS AT MACH NUMBER 4.04 OVER 6- AND 9-PERCENT-THICK SYMMETRICAL CIRCULAR-ARC AIRFOILS HAVING 30-PERCENT-CHORD TRAILING-EDGE FLAPS

By Edward F. Ulmann and Douglas R. Lord

SUMMARY

Pressure-distribution tests and schlieren photographs were made at a Mach number of 4.04 and Reynolds numbers of about 5.0×10^6 and 8.4×10^6 on 6- and 9-percent-thick symmetrical circular-arc airfoils having 30-percent-chord trailing-edge flaps. The experimental pressure distributions in the two-dimensional flow region at a Reynolds number of 5.0×10^6 showed some disagreements with the theoretical pressure distributions as a result of flow separation and shock - boundary-layer interaction. Due to the compensating nature of the pressure disagreements, the airfoil force and moment coefficients showed good agreement with the theoretically predicted values except for a reduction in flap effectiveness at angle configurations where flow separation became important. Increasing the Reynolds number from about 5.0×10^6 to about 8.4×10^6 in these tests decreased the extent of flow separation but had very little effect on the integrated airfoil force and moment coefficients. In general, viscous effects were found to be less important at the test Mach number and Reynolds numbers than at Mach numbers from 1.62 to 2.40 and a Reynolds number of 1.06×10^6.

INTRODUCTION

A program has been undertaken at the Langley Laboratory to determine the flow characteristics of rectangular wings having 6- and 9-percent-thick symmetrical circular-arc airfoil sections and trailing-edge flaps.

[redacted]

[redacted]

The chief object of the investigation was to discover some of the reasons for the discrepancies between experimental and theoretical control characteristics.

The results of low Reynolds number tests at Mach numbers of 1.62, 1.93, and 2.40 (references 1 and 2) showed that laminar separation caused a loss of control effectiveness at low flap deflections. The tests of reference 2 also showed that these seperation effects were reduced or eliminated by producing transition from laminar to turbulent boundary layer. The purposes of the present investigation are to evaluate, at a higher Mach number, the effects of flow separation, shock - boundary-layer interaction, and Reynolds number on the flow over these airfoils and to determine the applicability of some existing two-dimensional airfoil theories at a Mach number of 4.04.

The tests were made at a Mach number of 4.04 with a Reynolds number range from about 5.0×10^6 to 8.4×10^6, and included pressure measurements and schlieren photographs of the flow about the wings over a moderate range of angles of attack and flap deflections.

SYMBOLS

p_o	settling-chamber pressure
p_L	local static pressure on airfoil
p	stream static pressure
M	stream Mach number
R	Reynolds number, based on airfoil chord length
γ	ratio of specific heats for air, 1.4
q	dynamic pressure $\left(\frac{\gamma}{2} pM^2\right)$
P	pressure coefficient $\left(\frac{p_L - p}{q}\right)$
α	airfoil angle of attack
δ	flap deflection relative to airfoil chord, positive downward
x/c	distance from leading edge in chords

c	chord of airfoil
c_f	chord of flap
l	section lift
d_p	section pressure drag
d	section drag $\left(d_p + 0.003qc \text{ for skin friction}\right)$
$m_{.5}$	section pitching moment about midchord (positive when it tends to rotate the leading edge upward)
h	flap section hinge moment (positive when it tends to deflect the flap downward)
c_l	section lift coefficient $\left(l/qc\right)$
c_d	section drag coefficient $\left(d/qc\right)$
c_{d_p}	section pressure drag coefficient $\left(d_p/qc\right)$
$c_{m_{.5}}$	section pitching-moment coefficient about midchord $\left(m_{.5}/qc^2\right)$
c_h	section flap hinge-moment coefficient $\left(h/qc_f^2\right)$
c_{l_α}	variation of section lift coefficient with angle of attack
c_{m_α}	variation of section pitching-moment coefficient with angle of attack
$c_{l_{f_\delta}}$	variation of section flap lift coefficient with flap deflection
c_{m_δ}	variation of section pitching-moment coefficient with flap deflection
c_{h_δ}	variation of flap section hinge-moment coefficient with flap deflection
$\frac{\partial c_m}{\partial c_l}$	variation of section pitching-moment coefficient with section lift coefficient

[redacted]

$\frac{\partial \alpha}{\partial \delta}$ flap effectiveness factor $\left(\frac{\frac{\partial c_l}{\partial \delta}}{\frac{\partial c_l}{\partial \alpha}}\right)$

c.p. distance of airfoil center of pressure from leading edge of airfoil in chords, positive downstream

APPARATUS AND TESTS

Wind Tunnel

The tests were conducted in the Langley 9- by 9-inch Mach number 4 blowdown tunnel (fig. 1). The compressed-air system includes air dryers using activated alumina which dry the air to dew points from -20° F to -60° F at 300 pounds per square inch absolute. The test Reynolds number is changed by changing tunnel stagnation pressure, and runs of over 4 minutes duration are possible at the lowest running pressure. During test runs the stagnation pressure and temperature are continuously recorded on flight-type optical recorders. The air passes through four 16-mesh turbulence-damping screens in the settling chamber and then expands through fixed-geometry nozzle blocks and passes through a fixed second minimum into a diffuser. The cross-tunnel schlieren system uses two parabolic-front-surface reflectors 10 inches in diameter having 72-inch focal lengths. The light source is a 40,000-volt electric spark of about 1 microsecond duration.

Models

The pressure-distribution and schlieren models were made of steel and were of rectangular plan form with the tips cut off perpendicular to the chord plane. The models had 6- and 9-percent-thick circular-arc sections and 30-percent-chord true-contour trailing-edge flaps. The airfoil surfaces were finished to within 0.001 inch of the specified values and were polished smooth. The gap between the flap and the airfoil was 0.125 percent chord and was not sealed during the tests.

The pressure-distribution models had a 4-inch chord and a 5-inch span and were supported in the tunnel from a circular plate mounted flush with the side wall (fig. 2). The plate was rotated to change the angle of attack, which was measured by an inclinometer set on brackets on the outside of the plate. A rod from the flap root midchord section

extended through a sector cut in the angle-of-attack plate (fig. 2) and connected to a cover plate outside the tunnel, which rotated about the hinge pin extended. This cover plate was fitted with a bracket to mount the inclinometer. The angles of attack and the flap angles were set before each run in order to obtain the best accuracy in angle setting. The dimensions of the models and the orifice locations are given in figure 3. The spanwise location of the orifices was chosen so that they would be in a region of two-dimensional flow at all the test angles of attack and flap angles. The schlieren models had a 4-inch chord and an aspect ratio of 1 and were sting-supported, as shown in figure 4. An offset strut, having a 33-percent-thick diamond profile normal to the leading edge, swept back at 58°, extended from the lower surface of the wing to the sting support.

Tests

Tests were made to obtain pressure distributions at angles of attack from -2° to 10° and at flap angles ranging from about 16° to -16°. Test Reynolds numbers ranged from 5×10^6 to 8.8×10^6. Tests were run at humidities below 1×10^{-5} pounds of water vapor per pound of dry air. It is believed that this moisture content was low enough to eliminate any appreciable condensation effects from the data. The schlieren models were tested at approximately the same angles as the pressure-distribution models and the angles of attack under load were measured on the schlieren photographs. Due to the deflection of the rather long stings supporting the schlieren models, it was not feasible to obtain schlieren photographs at the same angles as the pressure distributions.

Precision of Data

Test-section conditions.- Tunnel calibration tests (see appendix) indicate that the Mach number in the region occupied by the model is 4.04 ± 0.02 and that flow conditions are suitable for aerodynamic testing.

Alinement of the models.- The probable error in alinement of the pressure-distribution models with the air stream is about ±0.10°. The probable error between angles of attack and between flap deflections of the pressure-distribution models as set before each run is ±0.03°.

Possible twisting of the pressure-distribution models was investigated by photographing the free ends of the wings under load and at no load. Measurements from the photographs of the 9-percent-thick model showed no twist of the main wing or the flap within the ±0.1° accuracy of the measurements. The measurements for the 6-percent-thick model

showed no measurable twist of the main wing but did show a maximum angular displacement of the flap tip of approximately 0.75° under maximum hinge moment. An analysis of the 6-percent pressure-distribution data indicated, however, that there was some twisting of the main wing. This twisting was noticeable only for positive pitching moments, probably because of the unsymmetrical internal construction of the model; therefore, the maximum inaccuracies in angle settings for the 6-percent-thick pressure-distribution model are probably about ±0.2° in angle of attack and ±0.75° in flap deflection. Corrections for twist were not applied to the data because of the approximations involved in determining the corrections throughout the angle range.

The probable error in the angle of attack of the schlieren models which was measured from the schlieren photographs is ±0.25°. The probable error between the flap angles of the schlieren models is ±0.1°.

Measurements and computations.- Measuring the airfoil pressures and obtaining the aerodynamic coefficients from such measurements involves certain errors which have been evaluated. The probable uncertainties of the coefficients and in the position of the center of pressure which would occur in these measurements and calculations are given in the following table:

c_l	c_{d_p}	$c_{m_{.5}}$	c_h	Center-of-pressure location (percent chord)
±0.005	±0.001	±0.001	±0.003	±1.5

The data for the 9-percent-thick airfoil are believed to be more accurate than indicated in the table because of the absence of any measurable aerodynamic twist.

RESULTS AND DISCUSSION

Pressure Results

General considerations.- Pressure distributions for both airfoils and schlieren flow photographs for the 9-percent-thick airfoil are presented for representative test-angle combinations in figures 5 to 7. The discussion will refer chiefly to the 9-percent data, since the flow characteristics are similar on both airfoils and are most easily seen on the thicker airfoil.

The theoretical pressure coefficients were computed by the shock-expansion method, which does not include the effects of flow separation, shock - boundary-layer interaction, or the reflection of expansions back to the airfoil by the leading-edge shock. For the 9-percent-thick airfoil (fig. 5) the experimental pressure distributions are for flap angles 0.75° more positive than the flap angles of the theoretical pressure distributions. Where a detailed comparison between the experimental and the theoretical pressure coefficients over the flap of the 9-percent-thick airfoil is made, the theoretical and experimental flap angles are the same. General comparisons can be made from figure 5, however, since the increments in pressure coefficient due to 0.75° flap deflection are very small throughout most of the flap-angle range.

The agreement between the experimental and the theoretical pressure distributions is, in general, good for both airfoils. Moderate disagreements were encountered on the high-pressure surfaces of the wings and flaps, as well as on the low-pressure surfaces of the wings just ahead of the hinge line when the deflected flap causes an increase in pressure on this surface.

Upper-surface flow conditions.- Flow separation on the upper or low-pressure surface was reported in tests of these same airfoils at lower supersonic Mach numbers (1.62, 1.93, and 2.40) and lower Reynolds numbers (0.55×10^6 and 1.07×10^6) in references 1 and 2. In the present tests increasing the Reynolds number from about 5×10^6 to about 8.4×10^6 completely eliminated separation on the upper surfaces of the airfoils at some angle configurations (figs. 8 and 9). It was found that the rearward movement of the separation point could also be brought about at a Reynolds number 5.0×10^6 by placing a roughness strip of No. 90 carborundum just behind the leading edge of the airfoil, thus causing the boundary layer to become turbulent. It is probable, therefore, that the rearward movement of the separation point, as shown in figure 9, is due to boundary-layer transition to turbulent flow at some point on the airfoil ahead of the flap hinge line as the Reynolds number is increased from 5.0×10^6 to 8.8×10^6.

The forward movement of the separation point on the upper surface with negatively increasing flap deflections (fig. 5) is the same movement which was observed at the lower Mach numbers and Reynolds numbers of reference 2.

Lower-surface flow conditions.- The experimental pressures on the lower or high-pressure surface of the airfoil ahead of the flap are somewhat more positive than the theoretical values. The magnitude of the disagreement increases along the chord and increases at each chordwise station with angle of attack. One factor which accounts for some of the difference between experiment and theory is the effect on the

[redacted]

pressure distributions of the interaction between the leading-edge shock and the expansion waves from the airfoil surface which is present in the actual flow. This interaction causes expansion waves to be reflected back onto the airfoil surface as compression waves, which in turn increase the pressures on the airfoil surface. These effects are neglected in the shock-expansion method of computing the pressure distributions. Reference 3 indicates that if this interaction is considered, the slope of the pressure-distribution curve at the airfoil leading edge would become increasingly lower than that predicted by the shock-expansion theory as the angle of attack is increased. However, the magnitude of this effect is not great enough to account for more than about one-third of the observed difference in slope between experiment and theory which exists at the airfoil leading edge.

The results of reference 1 showed that on the same airfoil at a Mach number of 1.62 and a Reynolds number of 1.07×10^6, flow separation and the accompanying forked shock occurred as far as 15 percent chord ahead of the wing-flap juncture on the airfoil lower surface at an angle of attack of 4.25° and flap angle of 13°. In contrast to this, the present tests did not show any evidence of separation of the flow ahead of the wing-flap juncture on the lower surface of the wing at corresponding angle configurations (figs. 5(d) and 5(e) and figs. 6(a) and 6(b)), which is believed due to the higher Reynolds numbers of these tests.

At positive angles of attack and positive flap angles, the pressures on the lower surface of the flap usually increase from a pressure lower than theoretical at the 73.25-percent-chord orifice to pressures higher than theoretical at the last three orifices on the flap (fig. 5). This gradual compression in the boundary layer occurs because the subsonic layer cannot support the sudden compression that occurs in the supersonic stream. The reasons for the pressures at the rearmost two or three orifices on the flap being higher than theoretical are as follows:

(1) The compressions at the wing-flap juncture start at a lower local Mach number and higher pressure than predicted by theory at the 70-percent station, except for $\alpha = 0^\circ$, and therefore would be expected to yield higher than theoretical pressures over the flap surface.

(2) The compressions occur gradually just outside the boundary layer because of the relieving effect of the boundary layer in the wing-flap juncture and would therefore according to shock theory result in a higher pressure than that predicted if a single shock were assumed.

The magnitude of these effects for a typical case is illustrated in figure 10. A theoretical shock compression through 16.75° from the experimental pressure on the wing just upstream of the wing-flap juncture,

followed by expansion over the flap surface, gives pressures over the flap about 10 percent higher than those given by a shock from the theoretical pressures at the 70-percent-chord station. An isentropic compression through 16.75° from the experimental pressures gives pressures over the flap about 20 percent higher than those given by a shock from the theoretical pressures at the 70-percent-chord station. The experimental pressures over the flap fall between these two curves, which is reasonable, since the compression is neither isentropic nor does it occur at a theoretical sharp corner.

Effect of airfoil thickness on the pressure distributions.- Figure 11 compares several typical pressure distributions for the 6-percent-thick airfoil with those for the 9-percent-thick airfoil at the same angle combinations. At the leading edge of the 9-percent airfoil the pressure coefficients on both surfaces are always higher than the corresponding pressure coefficients on the 6-percent airfoil due to the larger leading-edge angle of the 9-percent airfoil. From the leading edge back to the hinge line, the more rapid expansion along the surface of the 9-percent airfoil resulting from larger gradients of the surface causes the pressure coefficient to approach, and in some cases to become less than, that of the 6-percent airfoil. When an expansion of the flow is required at the hinge line, the pressure distributions on the flap surface are about the same for the two airfoils. However, when a compression occurs at the hinge line, the small differences in pressure coefficient and local Mach number ahead of the hinge cause a considerable difference in the final pressure coefficient obtained on the flap. In general, the pressure rise caused by a given flap deflection is higher on the 6-percent airfoil than on the 9-percent airfoil except possibly for cases involving separated flow.

Aerodynamic Characteristics

Section lift coefficient.- Plots of the section-lift-coefficient variation with angle of attack and flap deflection are presented in figure 12, from which it can be seen that the agreement between experiment and theory is best for low angles of attack and positive flap deflections. The largest increase in the experimental lift coefficients over the theoretical lift coefficients occurs at the higher angles of attack (6° and 10°) and the higher negative flap deflections. This increase occurs because of the previously discussed higher-than-theoretical pressures over the lower surfaces of both airfoils ahead of the flap, and because of flow separation on the upper surface ahead of the hinge line, which decreases the negative lift of the flap. An additional increment in the experimental lift coefficient over the theoretical lift for the 6-percent airfoil would be expected at the high angles of attack as a result of the model twist.

[redacted]

The flap-effectiveness factor $\frac{\partial \alpha}{\partial \delta}$ is presented in figure 13. The experimental values are generally in good agreement with theory except for combinations of positive angles of attack above 4° with negative flap deflections, where the experimental values are from 10 to 30 percent lower than the theoretical values. Examination of the lift curves of figure 12 shows that this is due to a lower-than-theoretical rate of change of lift with flap deflection at the stated angles, since the rate of change of lift with angle of attack is slightly higher than theoretical.

Section drag coefficients.- A section friction drag coefficient of 0.003 was added to all the pressure-drag coefficients obtained from the experimental and theoretical pressure distributions. This value was determined from unpublished force tests of a similar wing in the same tunnel. Any variation of friction drag with angle of attack was not determined.

The variation of the drag coefficient with angle of attack and flap deflection is presented in figure 14 for both the 6- and 9-percent-thick airfoils. The experimental section drag coefficients are generally in good agreement with the theory except at the higher flap deflections, where the experimental values are somewhat lower than the theory for both airfoils. This decrease in drag is the same as that previously noted in reference 4 at lower Mach numbers and is a result of the separation over a part of the rear portion of the airfoil, often over the whole flap low-pressure surface, which is accompanied by pressures higher than theoretically predicted.

Section lift-drag ratio.- The combination of higher lift and lower drag than theoretically predicted results in experimental lift-drag ratios which are generally higher than theory, as shown in figure 15. The maximum experimental lift-drag ratio for the 6-percent-thick airfoil is approximately 6.1, the theoretical maximum, 5.6. Maximum experimental lift-drag ratio obtained for the 9-percent-thick airfoil is 4.75, compared with a theoretical value of about 4.3.

Section pitching-moment coefficients.- The variations of section pitching-moment coefficient with section lift coefficient are presented in figure 16 for both airfoils. In general, the experimental data show good to excellent agreement with the theory. The small disagreements which exist are the results of flow separation, airfoil twist, and other effects which were discussed previously. Values of $\frac{\partial c_m}{\partial c_l}$ at $c_m = 0$ obtained from figure 16 are presented in figure 17 and show fairly good agreement with the theory.

[redacted]

The movement of the center of pressure with angle of attack for the 6- and 9-percent-thick airfoils computed from the section pitching-moment coefficient and section lift coefficient is shown in figure 18. The experimental center-of-pressure positions agree very well with the theoretical values at positive flap deflections but give fair to poor agreement at negative flap deflections where flow separation occurs. The center-of-pressure locations for the zero-flap-deflection conditions agree very closely with the values predicted by the shock-expansion theory (fig. 18).

Section flap hinge-moment coefficient.- Although the pressure distributions over the flaps for both airfoils showed considerable differences between experimental and theoretical pressures due to flow separation and shock - boundary-layer interaction, the plots of section flap hinge-moment coefficient against flap deflection (fig. 19) show good agreement between experiment and theory. This agreement is the result of the compensating nature of the disagreements pointed out in the pressure-distribution discussion. The agreement of the experimental section hinge-moment-coefficient data with theory is further shown in the curves of section hinge-moment-coefficient slopes plotted for $\delta = 0^\circ$ in figure 20.

The effect of Reynolds number on the aerodynamic characteristics.- The effect on the aerodynamic characteristics of increasing the Reynolds number of the flow from 5.1×10^6 to 8.0×10^6 for the 6-percent-thick airfoil and from 5.0×10^6 to 8.8×10^6 for the 9-percent-thick airfoil was in general negligible. Representative plots showing the maximum variation of the force and moment coefficients of the 6-percent-thick airfoil with Reynolds number are presented in figure 21. It should be noted that the data of these tests do not show - at Reynolds numbers of about 5.0×10^6 and 8.4×10^6 - any regions of control ineffectiveness such as those observed on the same airfoils at lower Mach numbers and Reynolds numbers (references 1 and 2); therefore, it may be concluded that at Mach numbers and Reynolds numbers in the range of these tests, trailing-edge flaps of the type investigated will be continuously effective through a range of angles of attack from 0° to 10° and a range of flap deflections from -16° to 16°.

Effect of airfoil thickness on the aerodynamic characteristics.- Some of the aerodynamic characteristics of the 6-percent-thick airfoil are compared with those of the 9-percent-thick airfoil in figure 22. The curves were chosen to cover the range of test and at the same time to show the most notable similarities and differences in the characteristics of the two airfoils.

The variation of section lift coefficient with flap deflection for 0°, 6°, and 10° angle of attack is presented in figure 22(a). The values for the two airfoils are very nearly the same except at angles

of attack of 6° and 10° for negative flap deflections, and at 0° angle of attack for positive flap deflections. In the first case, the 9-percent-thick airfoil has higher lifts because of the increased loadings over the forward portion of the airfoil and the decreased negative loading of the flap (figs. 5(d) and 5(e) and figs. 7(c) and 7(d)). In the second case, the 6-percent-thick airfoil gives higher lifts than the 9-percent airfoil because of the higher loading over the flap (figs. 11(a) and 11(b)).

The minimum pressure drag coefficients obtained for the two airfoils are in good agreement with the theoretical prediction that the minimum pressure drags should vary as the squares of the thickness ratios of the two airfoils. A comparison of the section-drag-coefficient variation with angle of attack for the two extreme flap deflections of the 6- and 9-percent-thick airfoils (fig. 22(b)) shows that, while the curves are very nearly the same for $\delta = 16°$, the 9-percent airfoil gives higher drag for $\delta = -16°$. The agreement in drag for the two airfoils at positive flap deflections is a result of the increased drag of the 6-percent flap over that of the 9-percent flap, which compensates for the lower drag of the forward portion of the 6-percent airfoil. For negative flap deflections, the pressure distributions over the flaps of the two airfoils are similar and the net effect is therefore to give a higher drag to the thicker airfoil, as predicted by the theory.

A comparison of the pitching-moment coefficients for the two airfoils at 0° and 10° angle of attack (fig. 22(c)) shows that the 9-percent-thick airfoil gives much larger changes in section pitching-moment coefficient with angle of attack than does the 6-percent-thick airfoil. This is due chiefly to differences in the center-of-pressure position on the two airfoils and is in agreement with theory.

The plot of section hinge-moment coefficient against angle of attack for flap deflections of -16°, 0°, and 16° (fig. 22(d)) shows that the experimental hinge moments change more rapidly with flap deflection on the 6-percent airfoil than on the 9-percent airfoil, as is predicted by the theory.

Comparison of experimental results with shock-expansion and second-order airfoil theories.- In table I a comparison is made between the experimental results at zero lift and the predictions of the shock-expansion theory and the Busemann second-order airfoil theory. The second-order theoretical values have been obtained by the methods of references 5 and 6. The equations of reference 5 are for symmetrical parabolic airfoils but can be applied to circular-arc airfoils, since the maximum differences in airfoil ordinates and surface angle between the 9-percent-thick symmetrical airfoils of each type are 0.014 percent chord and 0°5' of angle, respectively.

Referring to table I, it can be seen that the shock-expansion theory (used throughout this paper) usually gave more accurate predictions (within 11 percent of experimental values) of the aerodynamic characteristics of the airfoil at zero lift than did the second-order theory. The second-order theory becomes increasingly inaccurate as the airfoil thickness increases and is generally 20 to 30 percent low in its predictions of flap parameters, such as c_{m_δ} and c_{h_δ}. Besides better accuracy at zero lift, an obvious advantage of the shock-expansion theory is that it makes possible the accurate prediction of aerodynamic coefficients over the whole range of angles, as compared with the second-order theory.

CONCLUSIONS

An investigation, including pressure distributions and schlieren flow photographs, has been made of the flow characteristics over 6- and 9-percent-thick symmetrical circular-arc airfoils having 30-percent-chord trailing-edge flaps. Analysis of the results of these tests, which were conducted at a Mach number of 4.04 and at Reynolds numbers of about 5.0×10^6 and 8.4×10^6, indicated that:

1. The experimental pressure distributions at Reynolds number 5.0×10^6 showed good agreement with the pressure distributions computed by the shock-expansion theory, except over the flap surfaces and just ahead of the flap hinge line on the low-pressure side of the wing.

2. Due to the compensating nature of the disagreements between experiment and theory in the pressure distributions, the integrated section force and moment characteristics showed very good agreement with the theoretical characteristics, except for a reduction in flap effectiveness at angle configurations where flow separation over the flap became important.

3. Increasing the test Reynolds numbers from 5.0×10^6 to about 8.4×10^6 decreased the extent of the areas of separated flow but had little effect on the integrated force and moment coefficients.

4. The 6-percent-thick airfoil showed a smaller increment in section pitching-moment coefficient with changes in angle of attack and a larger increment in section flap hinge-moment coefficient with changes in flap deflection than did the 9-percent-thick airfoil.

5. In these tests the trailing-edge flaps were continuously effective throughout the angle range, whereas data obtained on the same

[redacted]

airfoils at Mach numbers from 1.62 to 2.40 and a Reynolds number of 1.06×10^6 showed regions of flap ineffectiveness caused by viscous effects.

Langley Aeronautical Laboratory
National Advisory Committee for Aeronautics
Langley Field, Va.

APPENDIX

TUNNEL CALIBRATION

Flow conditions in the test section of the Langley 9- by 9-inch Mach number 4 blowdown tunnel were determined from flow surveys made with $\frac{1}{16}$-inch-diameter flat-nosed total-pressure tubes and a 30° right circular cone. Figure 23 shows the location of the survey stations in the test section. Figure 24 presents the Mach numbers at these stations as determined from the ratio of test-section total pressure to settling-chamber pressure.

Transverse surveys were made at stations 3 to 10 at two values of absolute humidity, approximately 1×10^{-3} and 1×10^{-5} pounds of water vapor per pound of dry air. The only appreciable differences in indicated Mach number occurred at horizontal stations 9 and 10 (fig. 24(a)), and only the data for these stations for high and low humidities are shown. Repeat measurements at the same humidity checked within ±0.005 in Mach number. The average Mach number gradient in the flow direction for the low-humidity runs is 0.01 per inch over an 11-inch length. Mach numbers determined from pressures on a 30° cone and a wedge airfoil agreed well with the Mach numbers determined by the total-pressure measurements. In all cases the Mach number decreased in a downstream direction, probably because of the growth of the boundary layer, since the walls of the tunnel are parallel in the test section. The tunnel-wall boundary-layer thickness was found to be 0.8 inch on the tunnel floor and 1.1 inches on the side walls.

Figure 24(c) presents the results of six vertical surveys at three stations along the tunnel axis. Surveys were made at each station at stagnation pressures of 150 and 220 pounds per square inch absolute. No variation of Mach number with pressure could be determined. The surveys indicate the presence of weak shocks inclined downstream toward the tunnel axis from the tunnel ceiling and floor. No physical discontinuities could be observed in the nozzle-block contours which might cause such disturbances. These disturbances do not appear to have any measurable effect on the airfoil data, as indicated by the smooth airfoil pressure distributions obtained.

The error in airfoil pressure coefficient corresponding to the maximum Mach number variation found in the region occupied by the model is ±0.005. The effect of this error on the airfoil normal-force and moment coefficients is negligible. The bouyancy effect on the drag coefficient due to the Mach number difference is also negligible.

REFERENCES

1. Czarnecki, K. R., and Mueller, James. N.: Investigation at Mach Number 1.62 of the Pressure Distribution over a Rectangular Wing with Symmetrical Circular-Arc Airfoil Section and 30-Percent-Chord Trailing-Edge Flap. NACA RM L9J05, 1950.

2. Czarnecki, K. R., and Mueller, James N.: Investigation at Supersonic Speeds of Some of the Factors Affecting the Flow over a Rectangular Wing with Symmetrical Circular-Arc Section and 30-Percent-Chord Trailing-Edge Flap. NACA RM L50J18, 1951.

3. Munk, M. M., and Prim, R. C.: Surface-Pressure Gradient and Shock-Front Curvature at the Edge of a Plane Ogive with Attached Shock Front. Jour. Aero. Sci., vol. 15, no. 11, Nov. 1948, pp. 691-695.

4. Ferri, Antonio: Experimental Results with Airfoils Tested in the High-Speed Tunnel at Guidonia. NACA TM 946, 1940.

5. Morrissette, Robert R., and Oborny, Lester F.: Theoretical Characteristics of Two-Dimensional Supersonic Control Surfaces. NACA RM L8G12, 1948.

6. Ferri, Antonio: Elements of Aerodynamics of Supersonic Flows. The Macmillan Co., 1949.

[redacted]

TABLE I

COMPARISON OF EXPERIMENTAL DATA AT ZERO LIFT WITH THE SHOCK-EXPANSION THEORY AND THE BUSEMANN SECOND-ORDER AIRFOIL THEORY AT MACH NUMBER 4

Aerodynamic characteristics	Experimental results		Shock-expansion theory		Busemann second-order theory (references 5 and 6)	
	6 percent	9 percent	6 percent	9 percent	6 percent	9 percent
c_{l_α}	0.020	0.020	0.018	0.020	0.018	0.018
c_{d_p}	0.0045	0.011	0.0050	0.011	0.0050	0.011
c_{m_α}	0.0016	0.0022	0.0014	0.0021	0.0016	0.0026
c_{m_δ}	-0.0012	-0.00092	-0.0012	-0.00098	-0.0011	-0.00068
c_{h_δ}	-0.0060	-0.0042	-0.0057	-0.0041	-0.0049	-0.0028
$c_{l_{f\delta}}$	0.0037	0.0027	0.0038	0.0030	0.0032	0.0022
$c.p._{\frac{\delta}{\alpha}=1}$	0.49	0.45	0.49	0.45	0.47	0.41

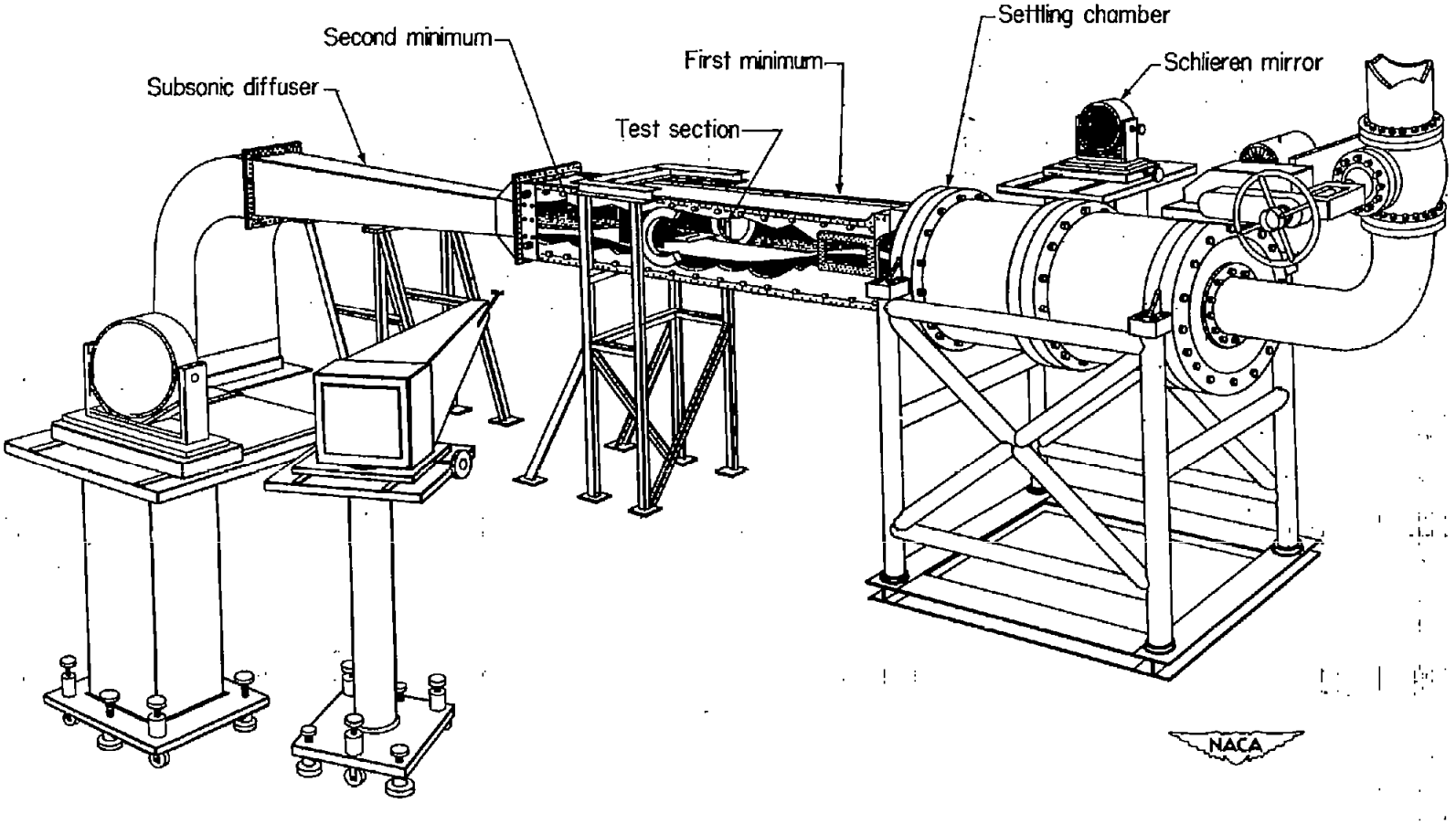

Figure 1.- Schematic view of the Langley 9- by 9-inch Mach number 4 blowdown tunnel with tunnel side wall cut away.

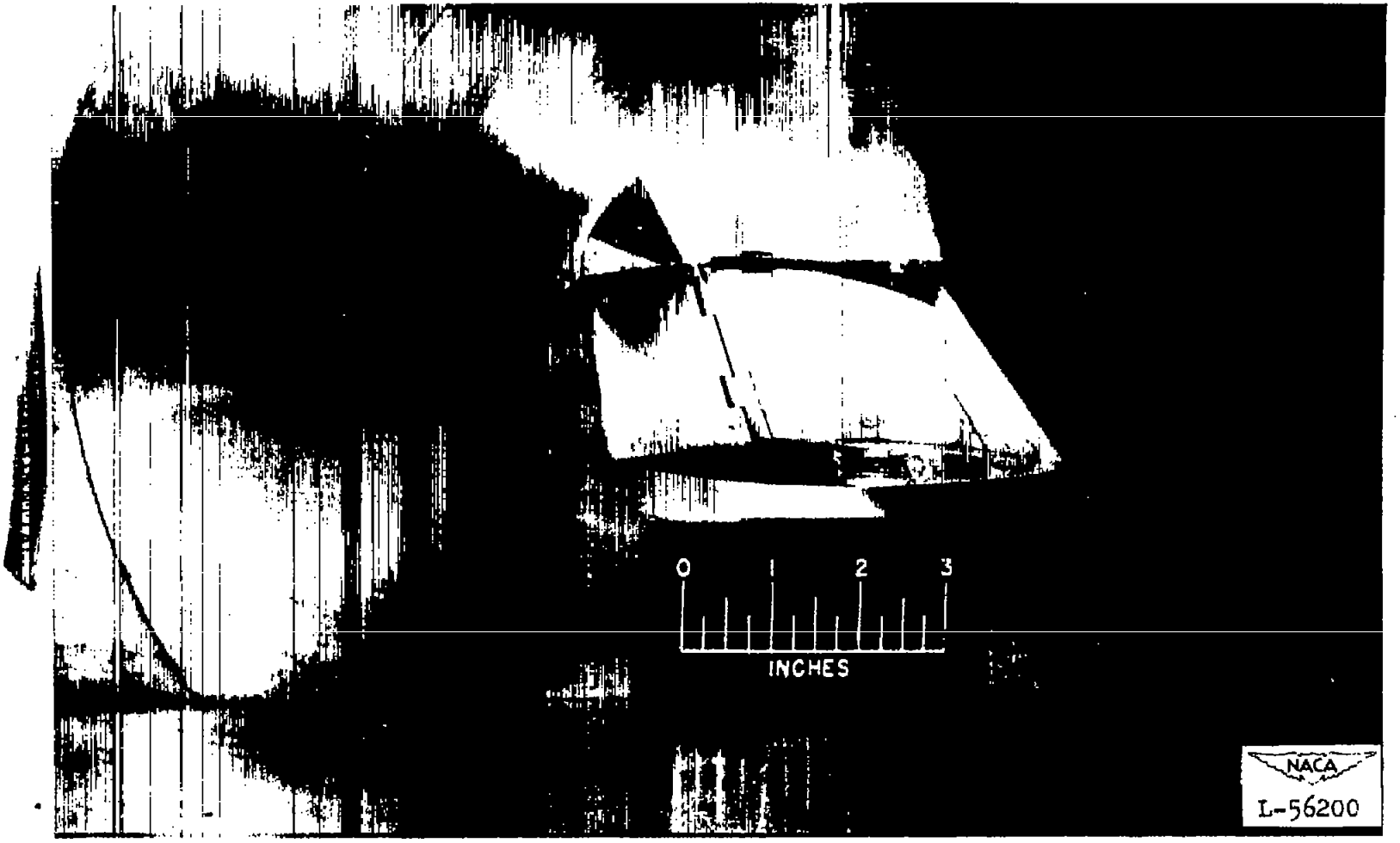

Figure 2.- Pressure-distribution model mounted in the test section of the Langley 9- by 9-inch Mach number 4 blowdown tunnel.

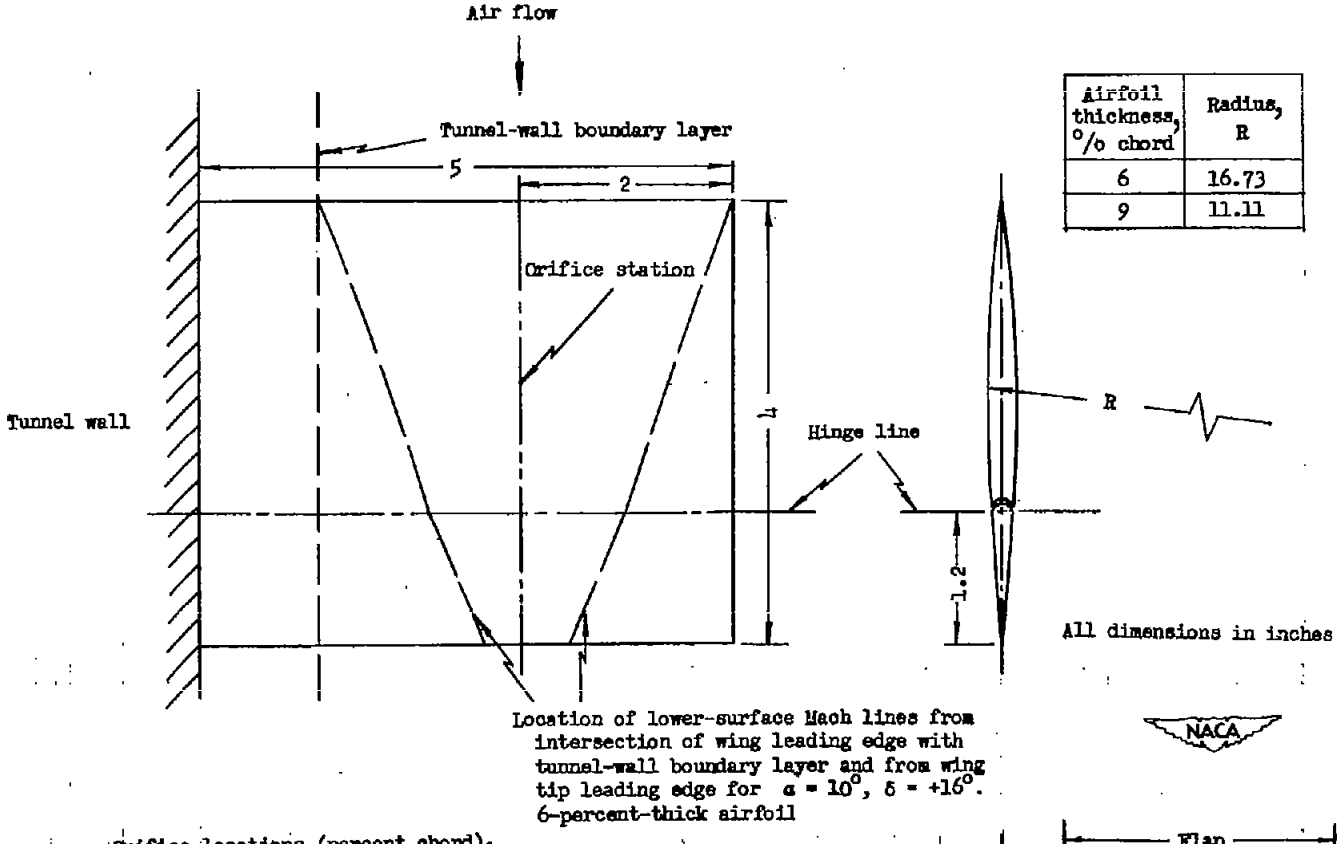

Airfoil thickness, % chord	Radius, R
6	16.73
9	11.11

Orifice locations (percent chord):

Model	Orifice No.	1	2	3	4	5	6	7	8	9	10	Flap 11	12	13	14
6%	Upper surface	9.25	12.50	18.75	25.00	31.25	37.50	43.75	50.00	56.25	62.50	72.50	80.00	86.25	92.50
6%	Lower surface	5.25	12.50	18.75	25.00	31.25	37.50	43.88	50.13	56.25	62.50	73.50	79.50	86.25	92.50
9%	Both surfaces	6.25	12.50	18.75	25.00	31.25	37.50	43.75	50.00	56.25	62.50	73.75	80.00	86.25	92.50

Figure 3.- Model dimensions and orifice locations for the 6- and 9-percent-thick symmetrical circular-arc pressure distribution models with trailing-edge flaps.

Figure 4.- Schlieren model on sting support in the test section of the Langley 9- by 9-inch Mach number 4 blowdown tunnel.

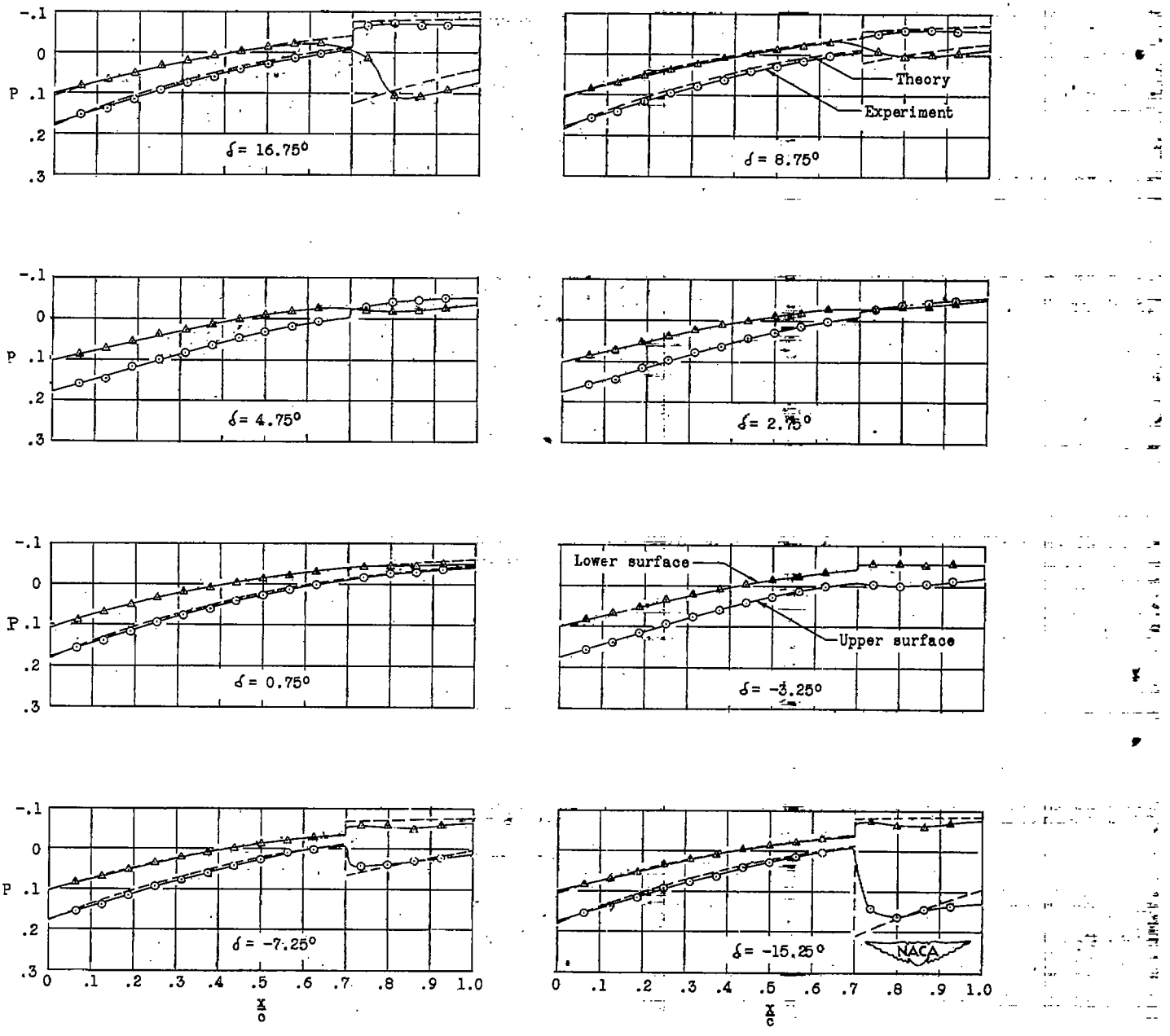

(a) $\alpha = -2^{\circ}$.

Figure 5.- The effect of flap deflection on the experimental and theoretical pressure distributions in a two-dimensional flow region on a 9-percent-thick symmetrical circular-arc airfoil. M, 404; R, 5.0×10^6.

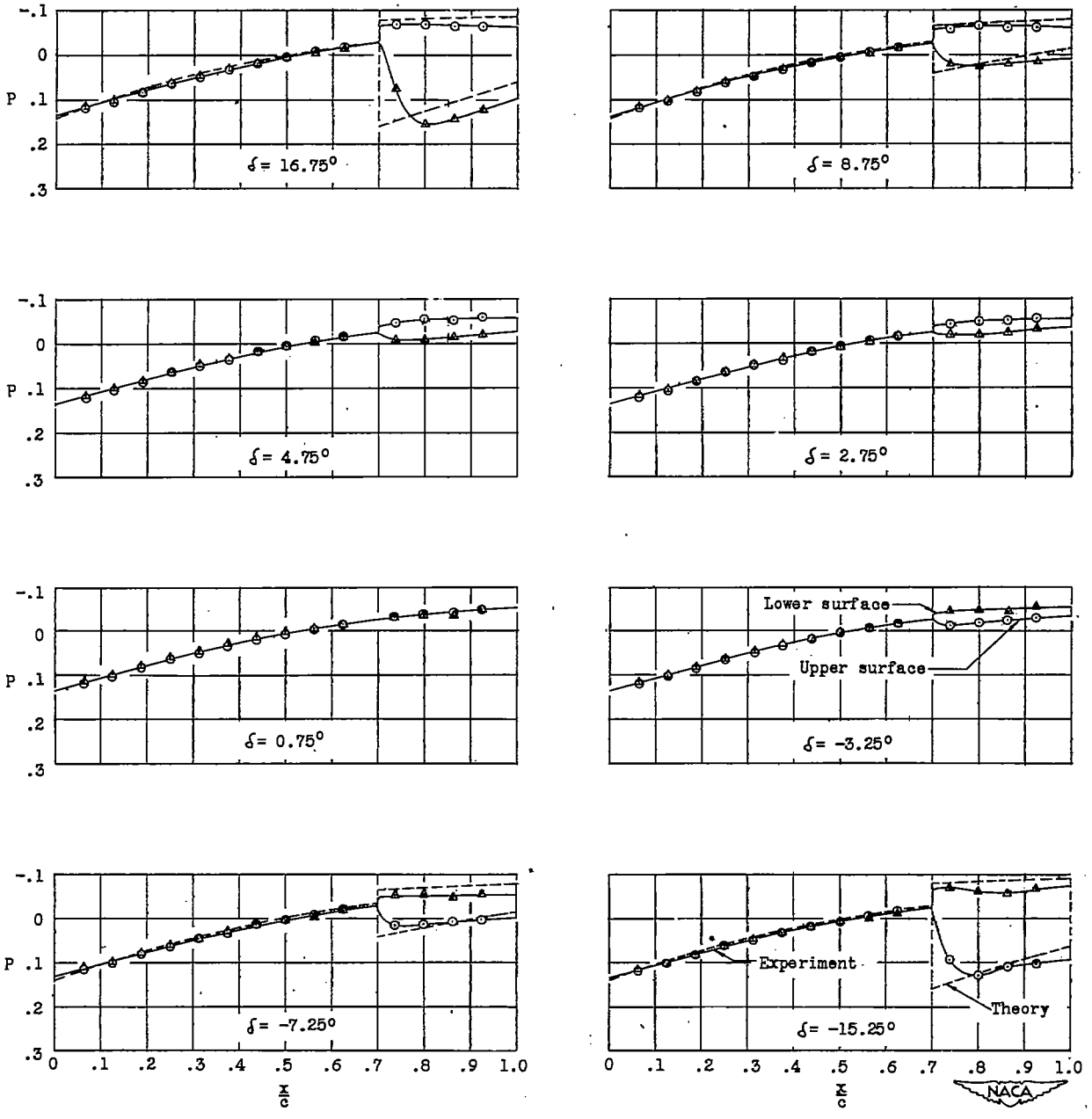

(b) $\alpha = 0^{\circ}$.

Figure 5.- Continued.

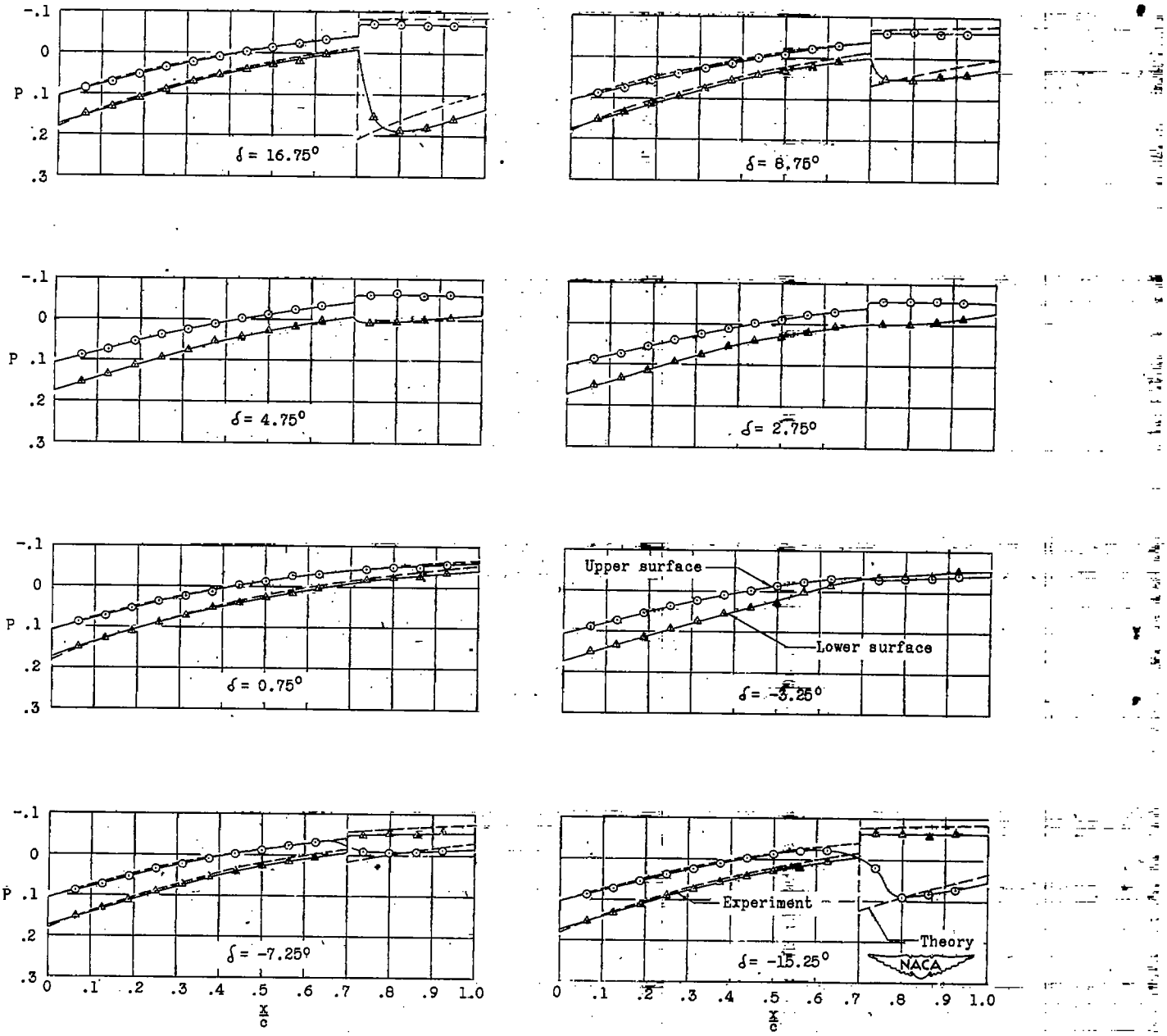

(c) $\alpha = 2^{\circ}$.

Figure 5.- Continued.

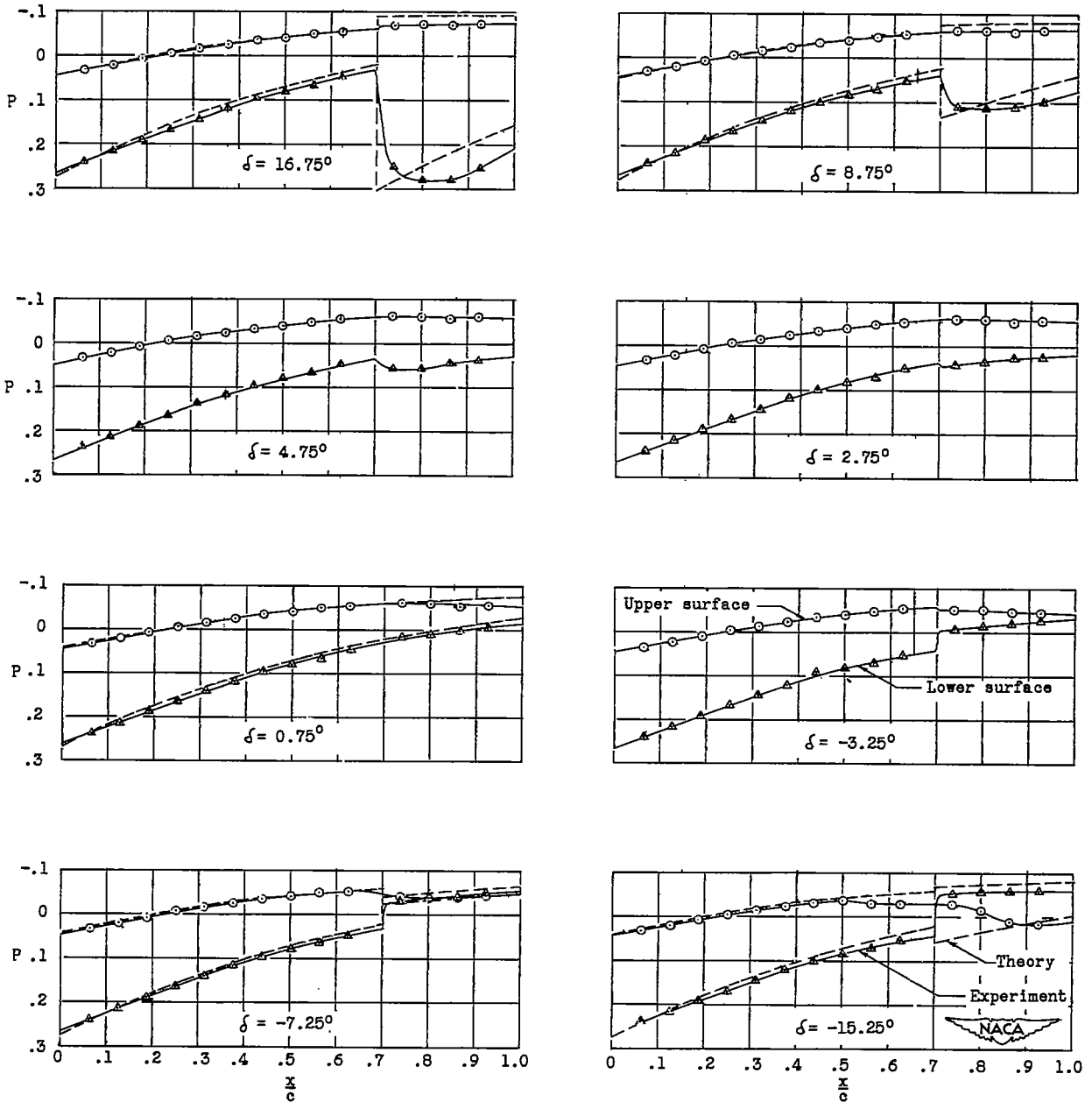

(d) $\alpha = 6^\circ$.

Figure 5.- Continued.

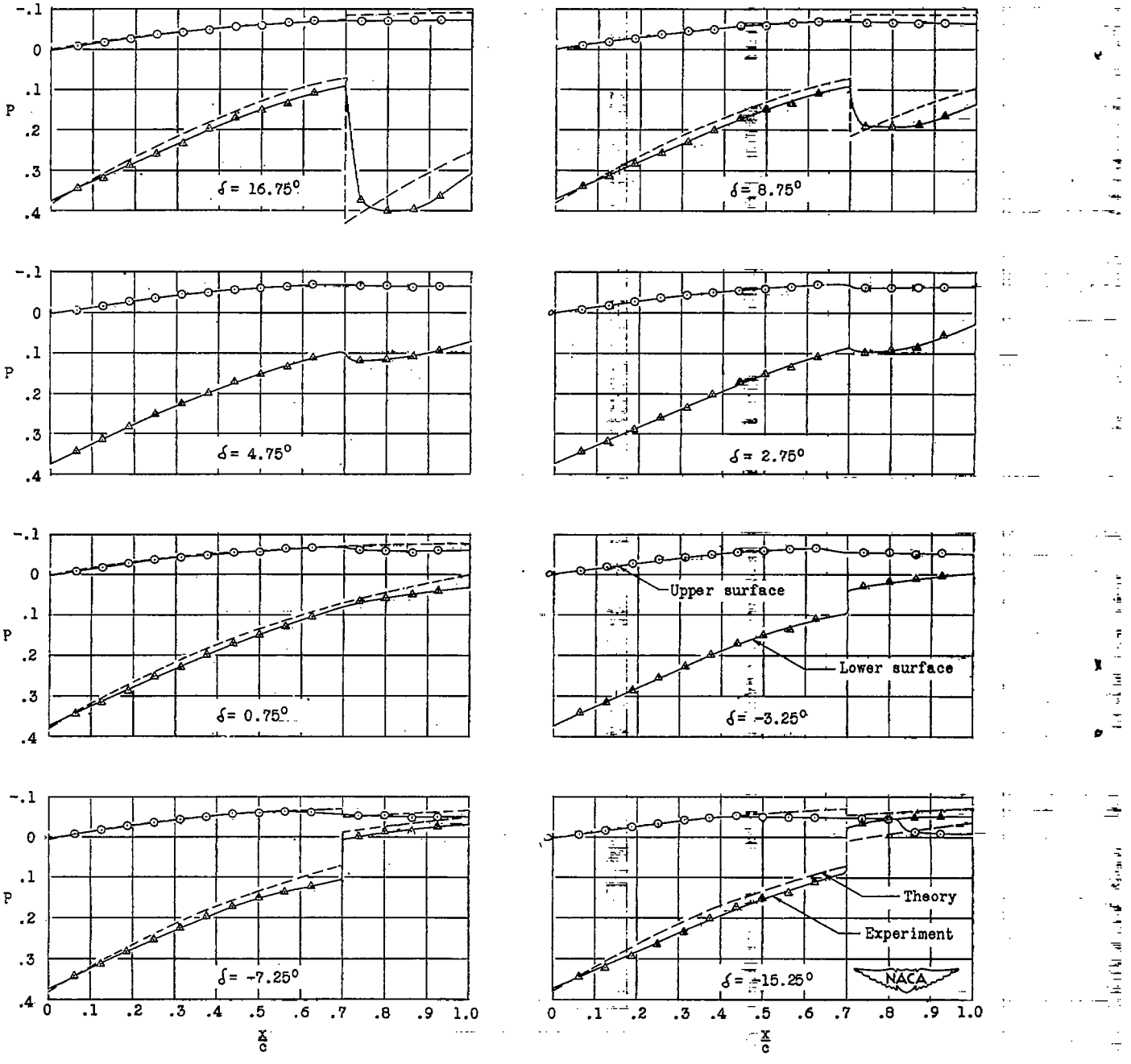

(e) $\alpha = 10^{\circ}$.

Figure 5.- Concluded.

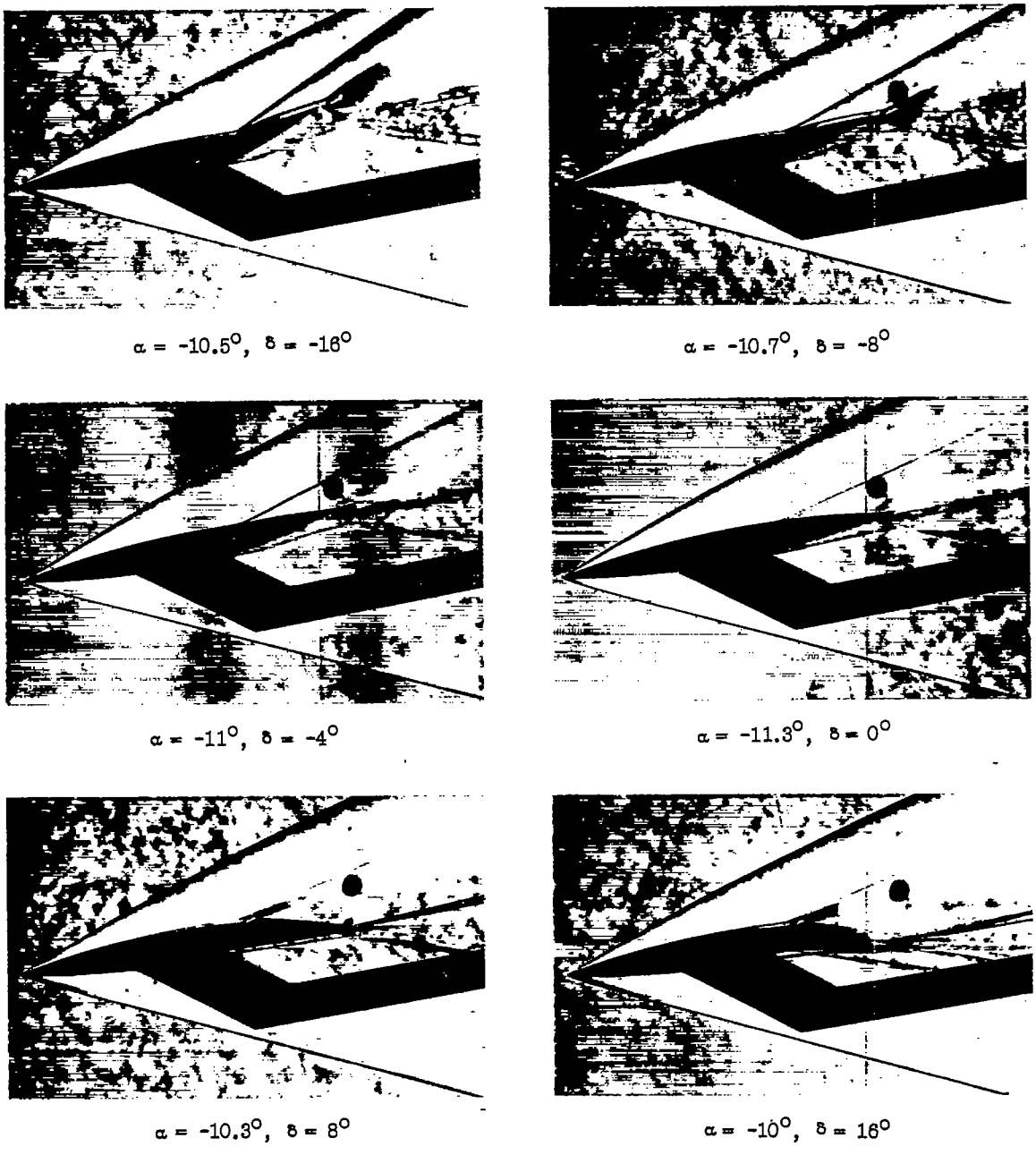

(a) $\alpha \approx -10°$.

NACA L-70751

Figure 6.- Schlieren photographs showing the effects of flap deflection on the flow around an aspect-ratio-1 wing having a 9-percent-thick symmetrical circular-arc airfoil section. Vertical knife edge. M, 4.04; R, 5×10^6.

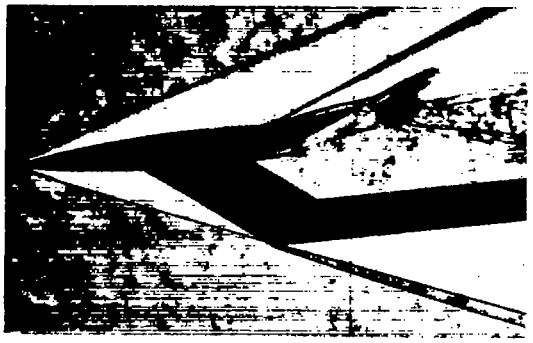

$\alpha = -6.5^\circ$, $\delta = -16^\circ$

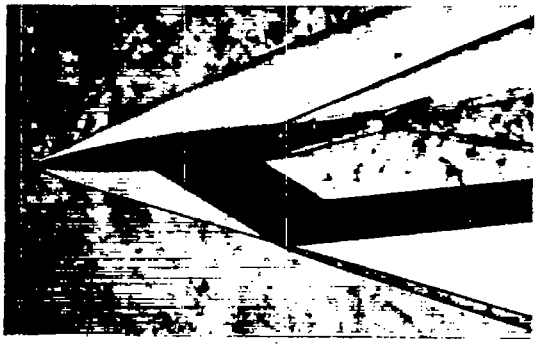

$\alpha = -6.5^\circ$, $\delta = -8^\circ$

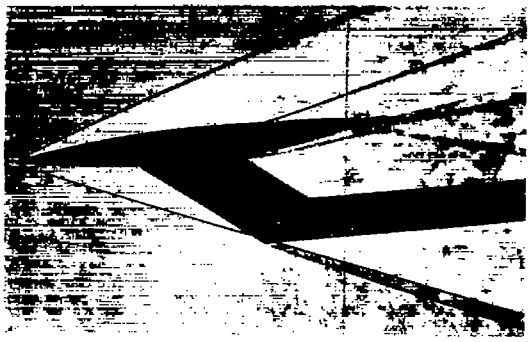

$\alpha = -6.0^\circ$, $\delta = -4^\circ$

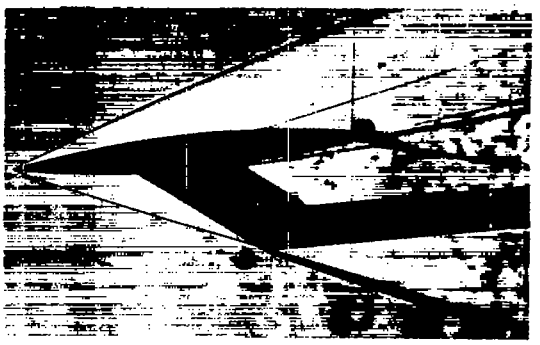

$\alpha = -6.5^\circ$, $\delta = 0^\circ$

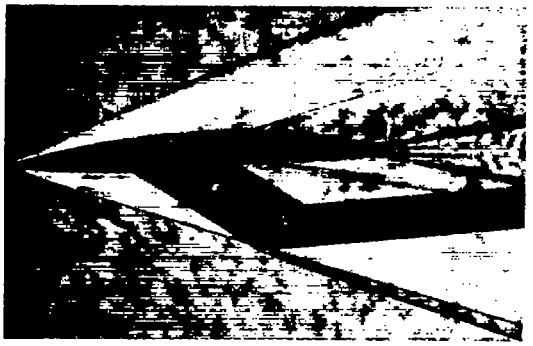

$\alpha = -6.0^\circ$, $\delta = 8^\circ$

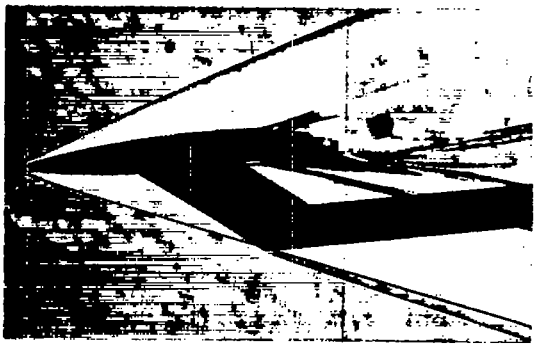

$\alpha = -6.3^\circ$, $\delta = 16^\circ$

(b) $\alpha \approx -6^\circ$.

Figure 6.- Continued.

NACA

L-70752

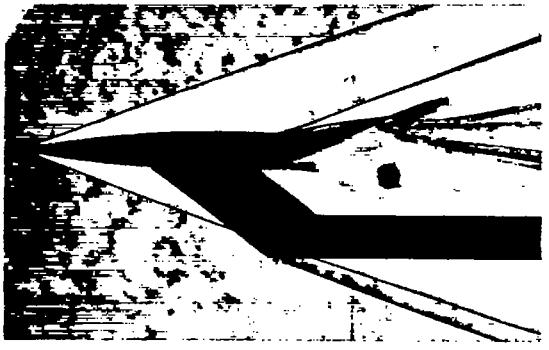

$\alpha = 0.2^\circ$, $\delta = -16^\circ$

$\alpha = 0.0^\circ$, $\delta = -8^\circ$

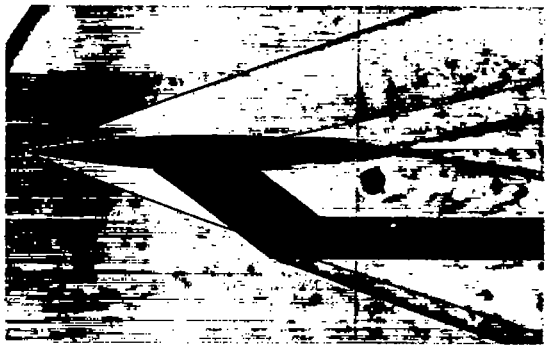

$\alpha = 0.0^\circ$, $\delta = -4^\circ$

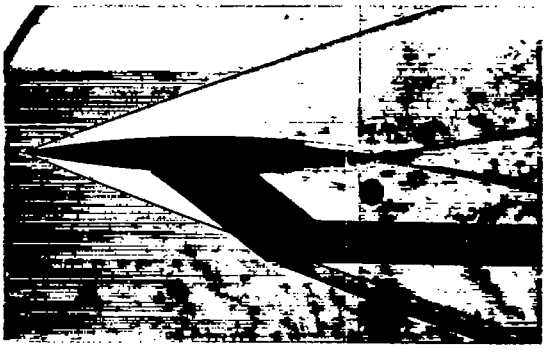

$\alpha = 0.3^\circ$, $\delta = 0^\circ$

$\alpha = 0.7^\circ$, $\delta = 8^\circ$

$\alpha = 0.5^\circ$, $\delta = 16^\circ$

(c) $\alpha \approx 0^\circ$.

Figure 6.- Continued.

NACA L-70753

$\alpha = 8.0^\circ$, $\delta = -16^\circ$

$\alpha = 7.0^\circ$, $\delta = -8^\circ$

$\alpha = 6.4^\circ$, $\delta = -4^\circ$

$\alpha = 7.2^\circ$, $\delta = 0^\circ$

$\alpha = 7.8^\circ$, $\delta = 8^\circ$

$\alpha = 8.0^\circ$, $\delta = 16^\circ$

(d) $\alpha \approx 7^\circ$.

NACA

L-70754

Figure 6.- Continued.

$\alpha = 10.8^\circ$, $\delta = -16^\circ$

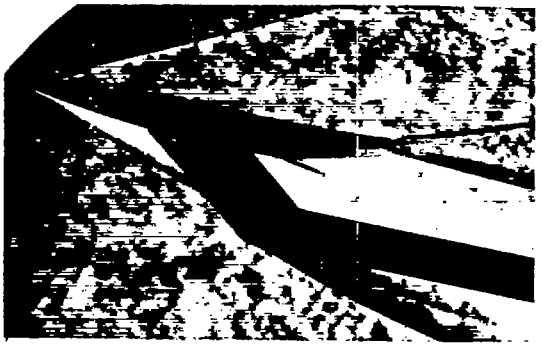

$\alpha = 11.2^\circ$, $\delta = -8^\circ$

$\alpha = 11.3^\circ$, $\delta = -4^\circ$

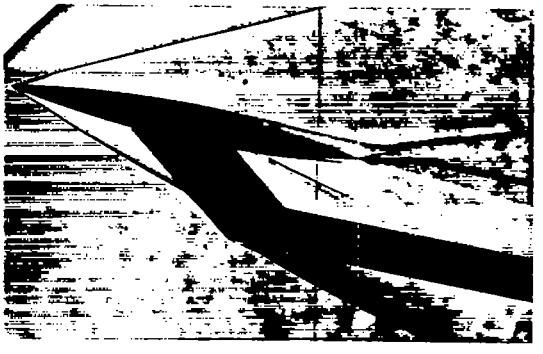

$\alpha = 11.0^\circ$, $\delta = 0^\circ$

$\alpha = 11.7^\circ$, $\delta = 8^\circ$

$\alpha = 12.0^\circ$, $\delta = 16^\circ$

(e) $\alpha \approx 11^\circ$.

Figure 6.- Concluded.

NACA

L-70755

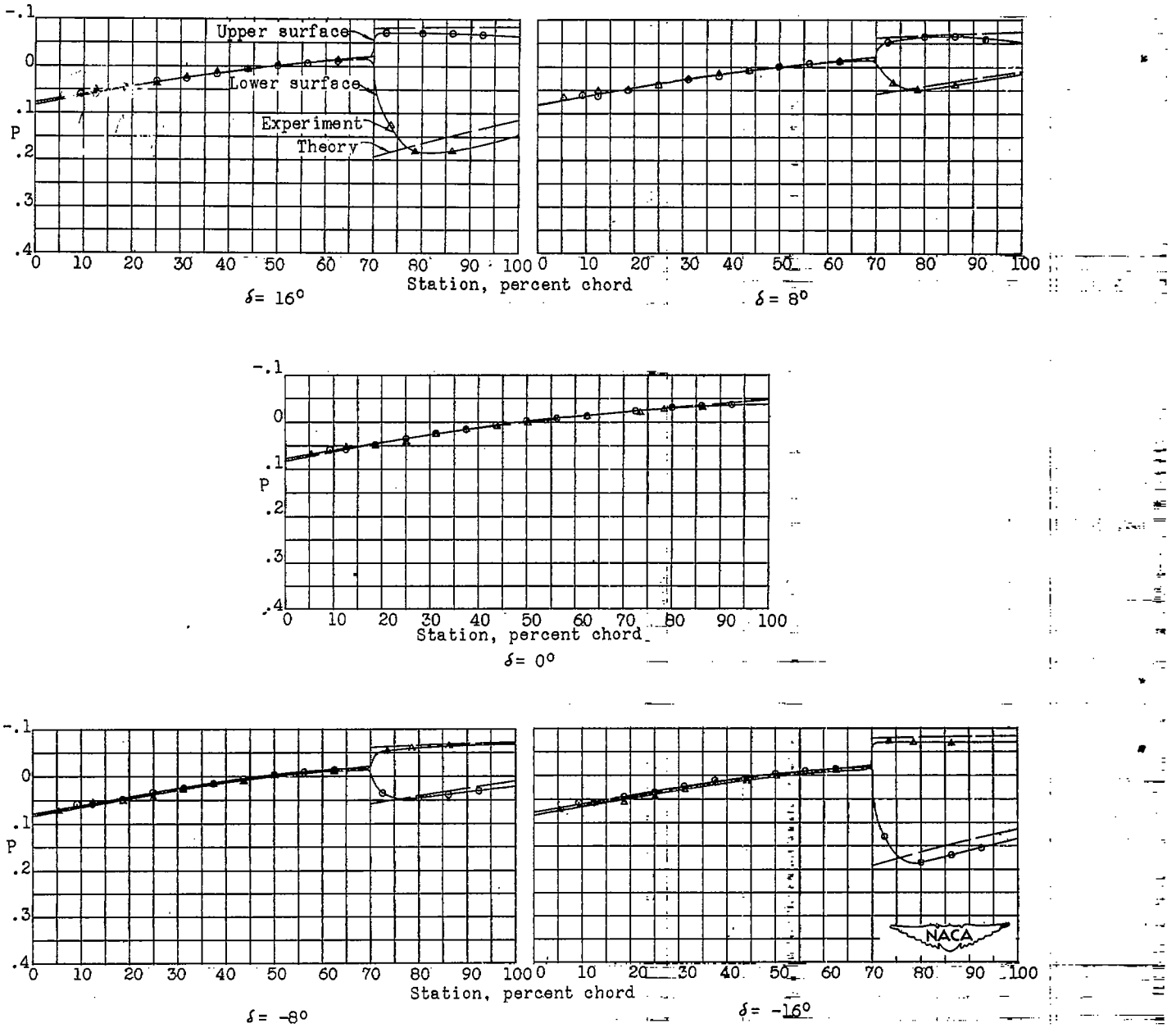

(a) $\alpha = 0^{\circ}$.

Figure 7.- The effect of flap deflection on the experimental and theoretical pressure distributions in a two-dimensional flow region on a 6-percent-thick symmetrical circular-arc airfoil. M, 4.04; R, 5.1×10^6.

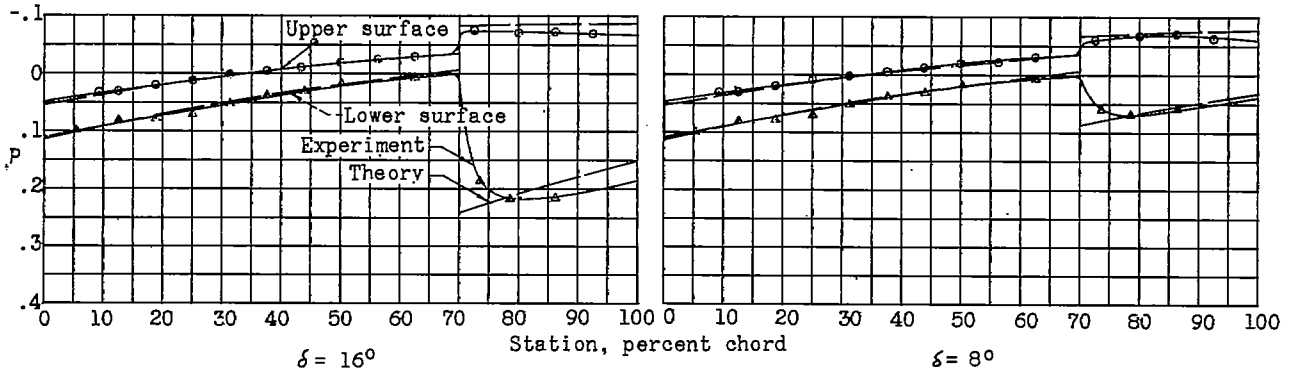

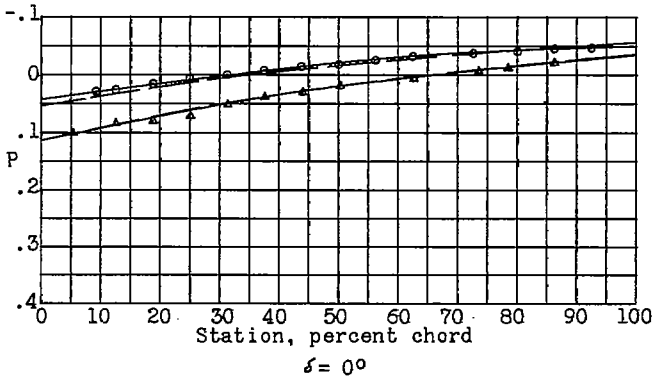

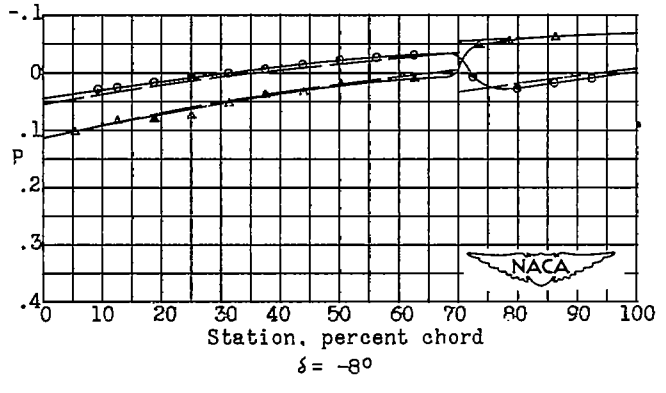

(b) $\alpha = 2^{\circ}$.

Figure 7.- Continued.

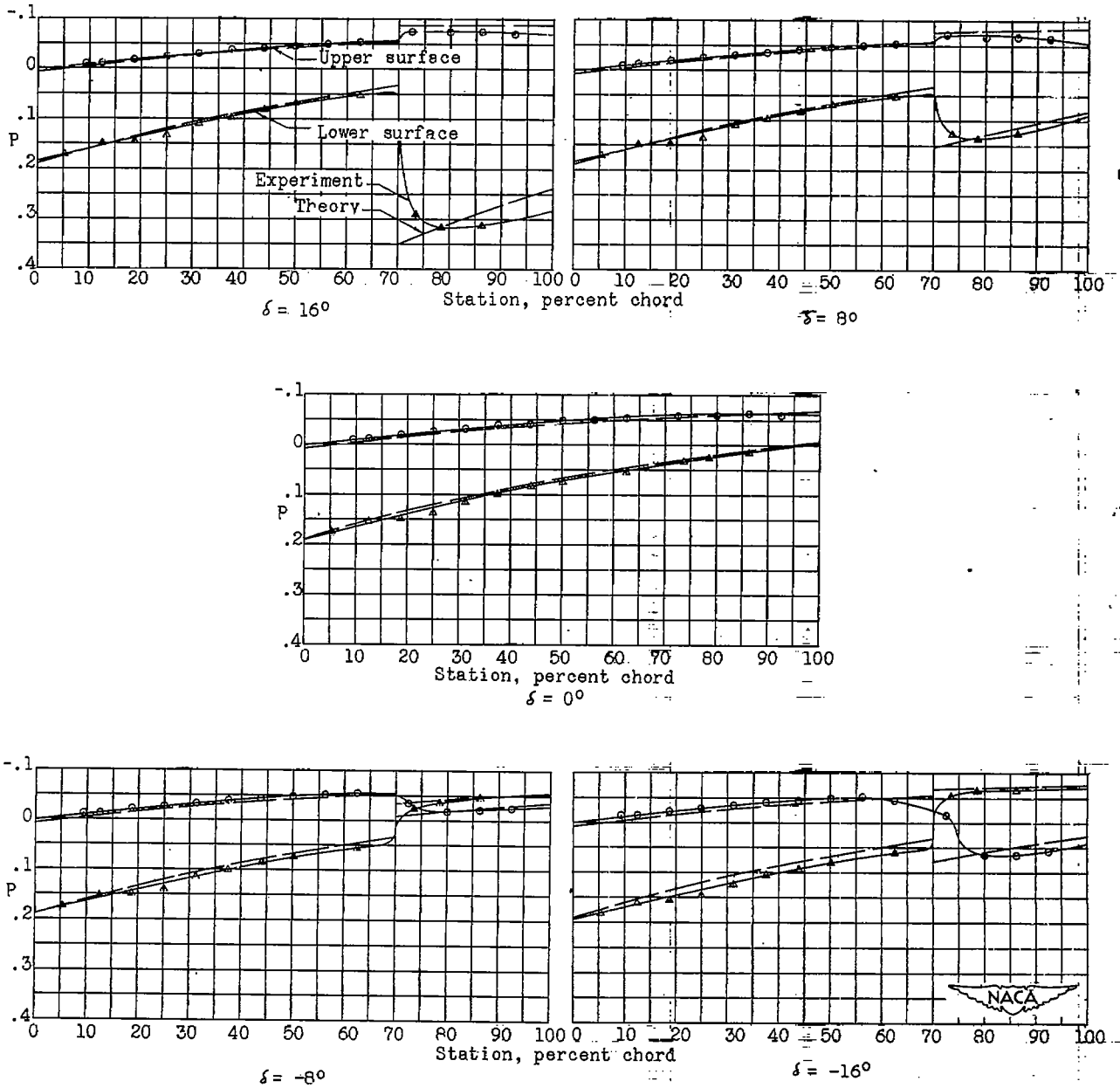

(c) $\alpha = 6^{\circ}$.

Figure 7.- Continued.

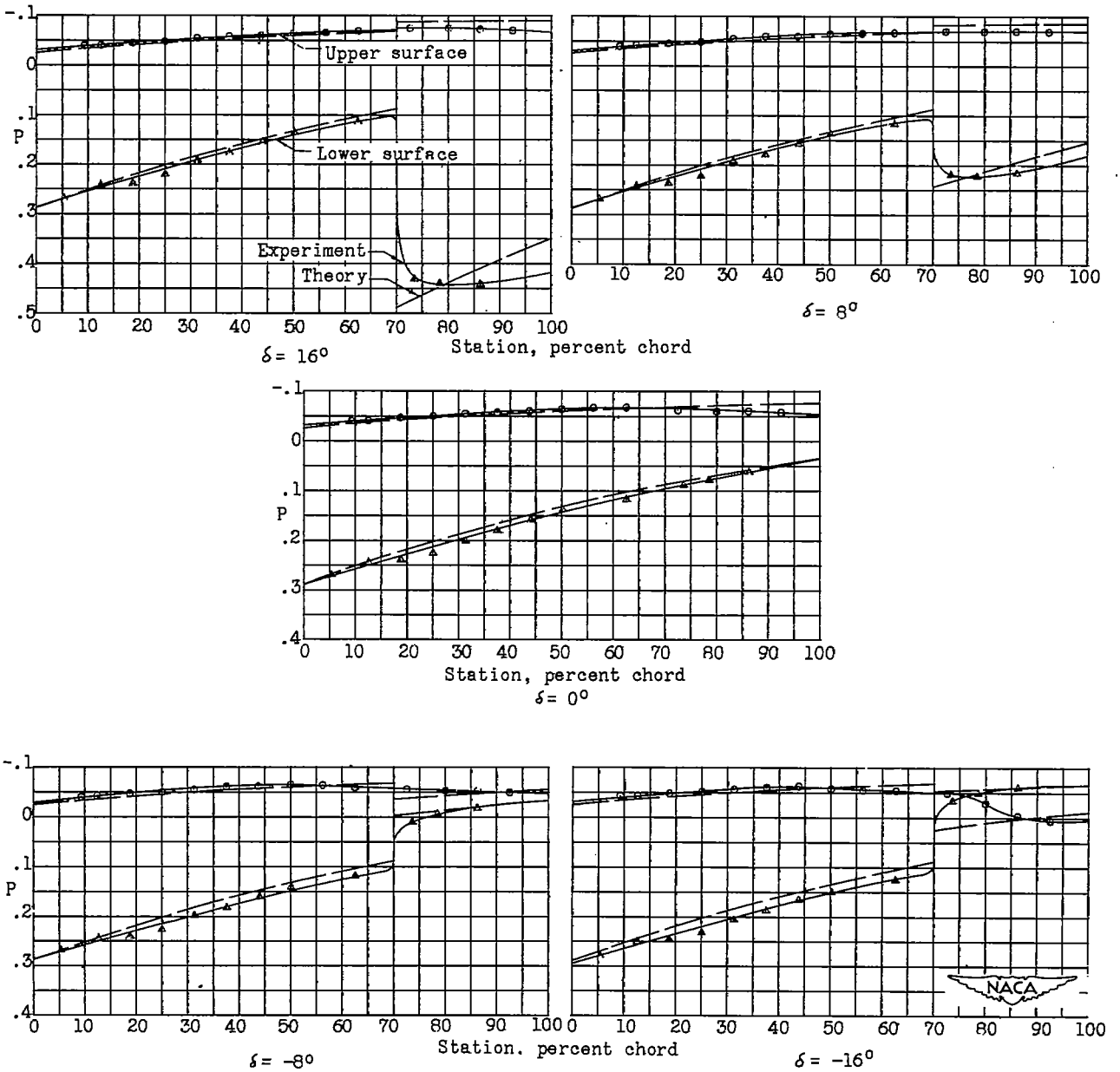

(d) $\alpha = 10^{\circ}$.

Figure 7.- Concluded.

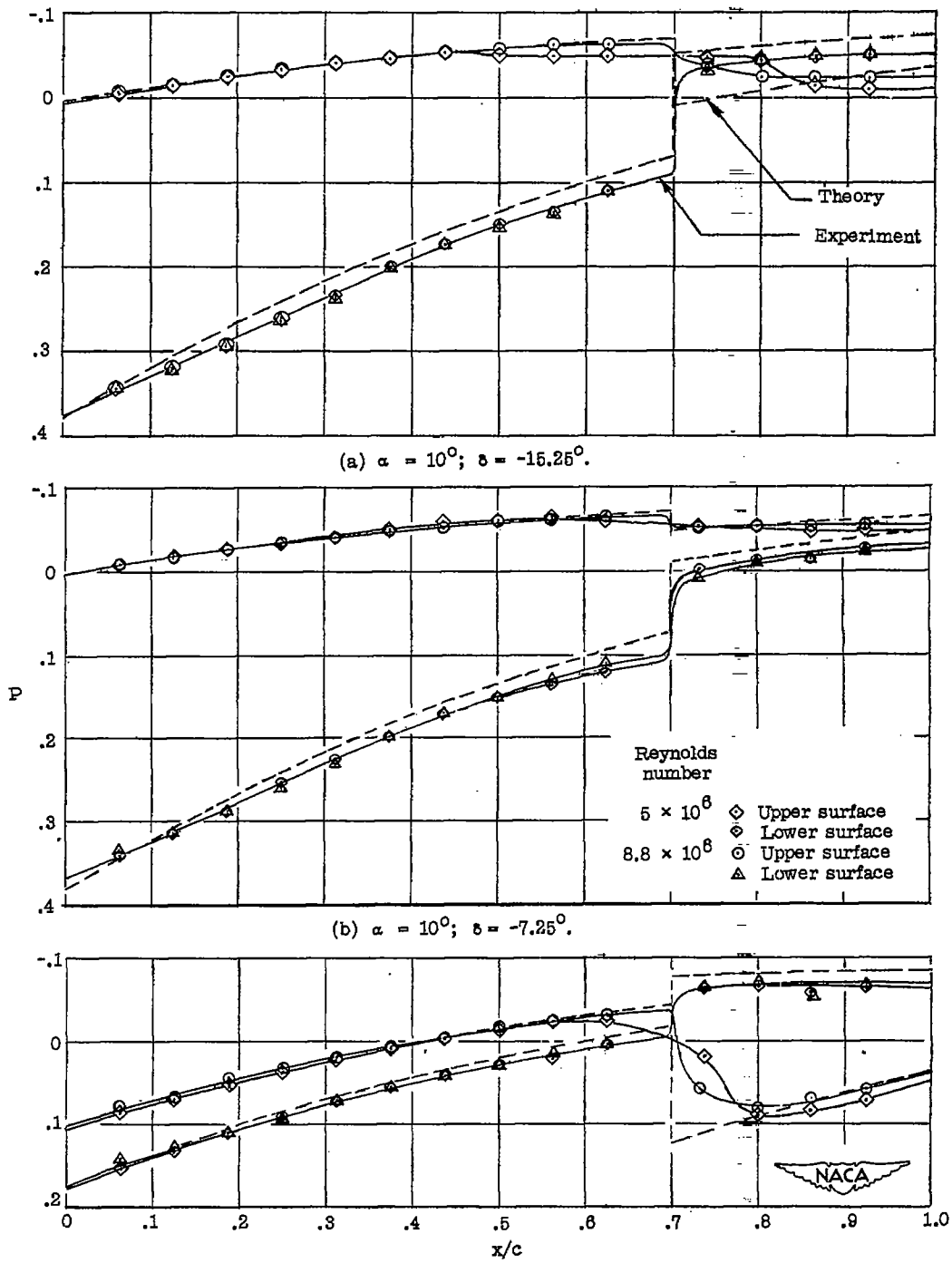

Figure 8.- Effect of Reynolds number on experimental pressure distributions in a two-dimensional region on a 9-percent-thick symmetrical circular-arc airfoil. M, 4.04.

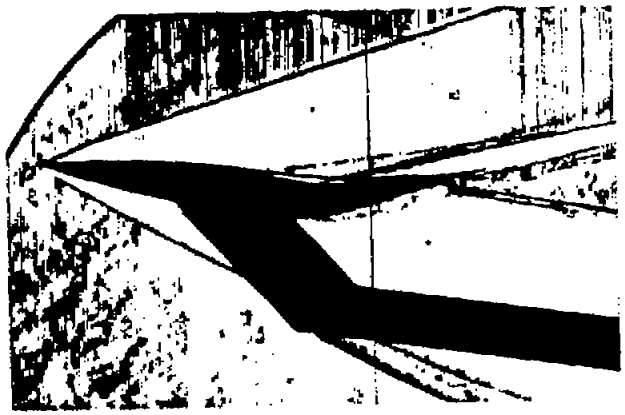

(a) $R = 5.0 \times 10^6$; $\alpha = 8.0^\circ$; $\delta = -16^\circ$.

(b) $R = 8.8 \times 10^6$; $\alpha = 7.5^\circ$; $\delta = -16^\circ$.

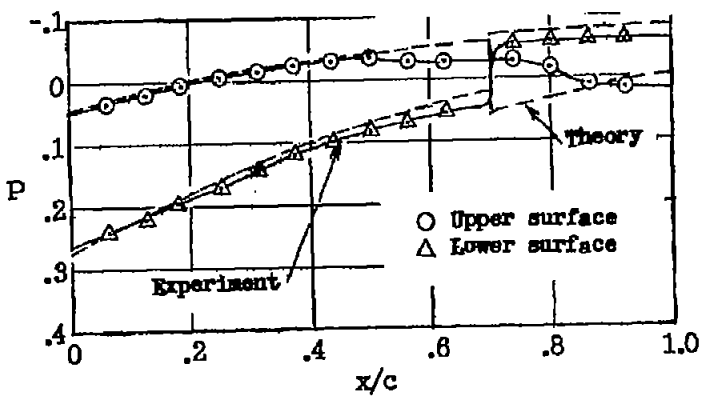

(c) $R = 5.0 \times 10^6$; $\alpha = 6.0^\circ$; $\delta = -15^\circ 15'$.

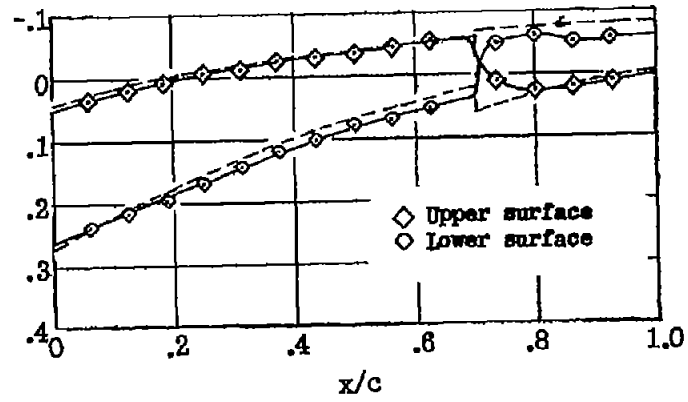

(d) $R = 8.8 \times 10^6$; $\alpha = 6.0^\circ$; $\delta = -15^\circ 15'$.

Figure 9.- The change in flow conditions with increasing Reynolds number on the 9-percent-thick circular-arc airfoil as seen in schlieren photographs and pressure distributions. M, 4.04.

NACA L-70756

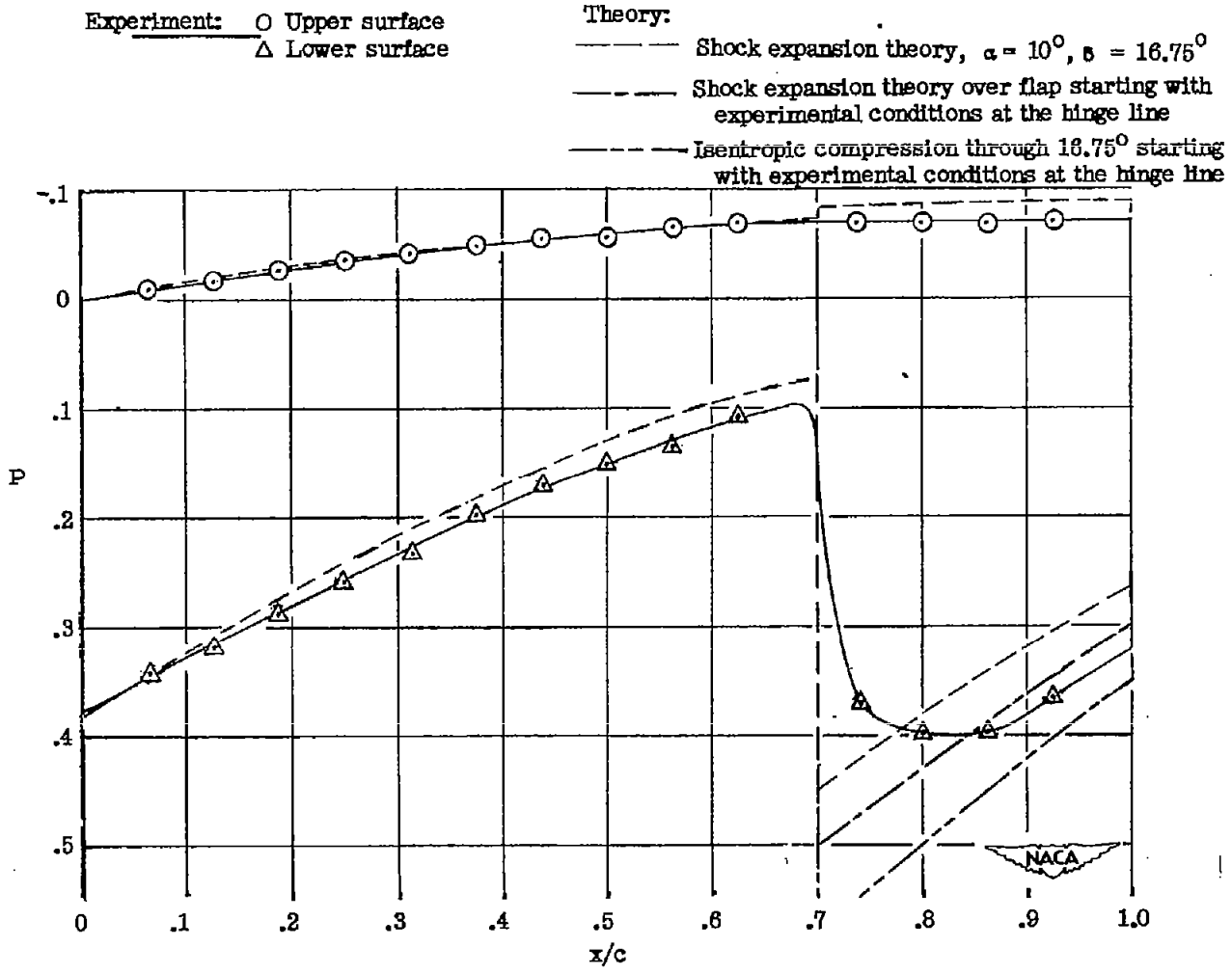

Figure 10.- Experimental and theoretical pressure distributions in a region of two-dimensional flow on a 9-percent-thick symmetrical circular-arc airfoil at $\alpha = 10^{\circ}$ and $\delta = 16^{\circ}45'$.

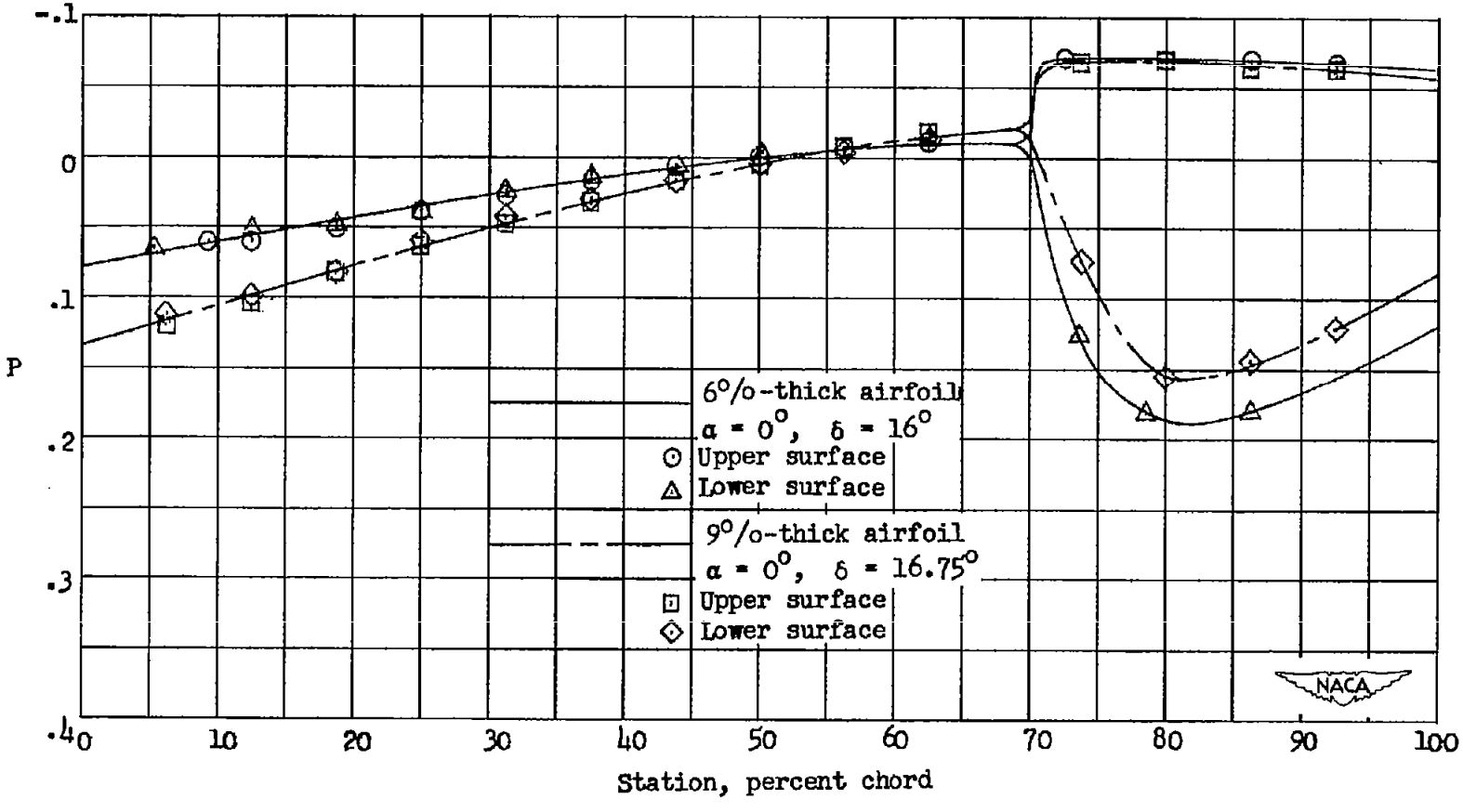

(a) $\alpha = 0^{\circ}$.

Figure 11.- The effect of changing thickness ratio on the pressure distributions over circular-arc airfoils with 30-percent-chord trailing-edge flaps. M, 4.04; R, 5×10^6.

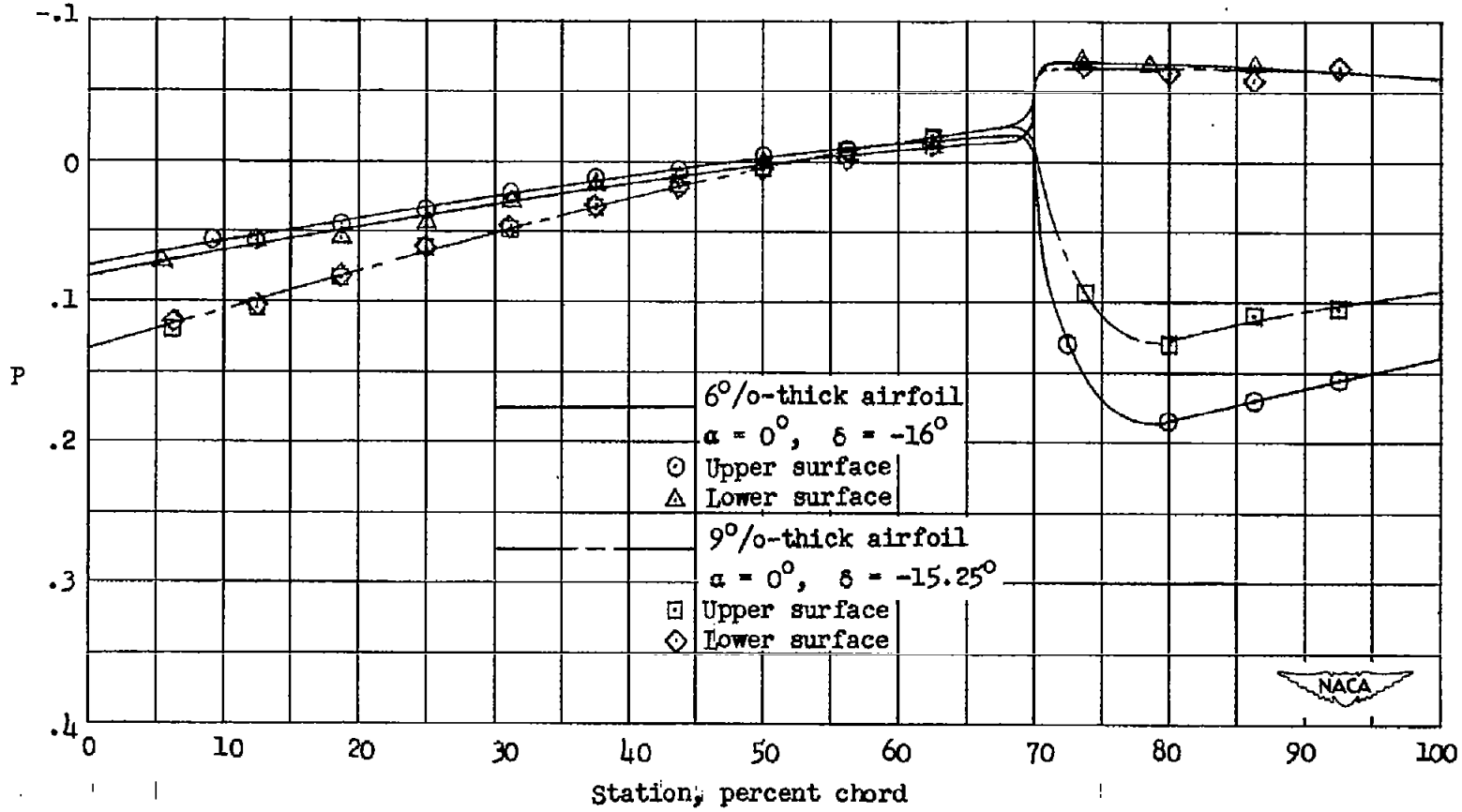

(b) $\alpha = 0°$.

Figure 11.- Continued.

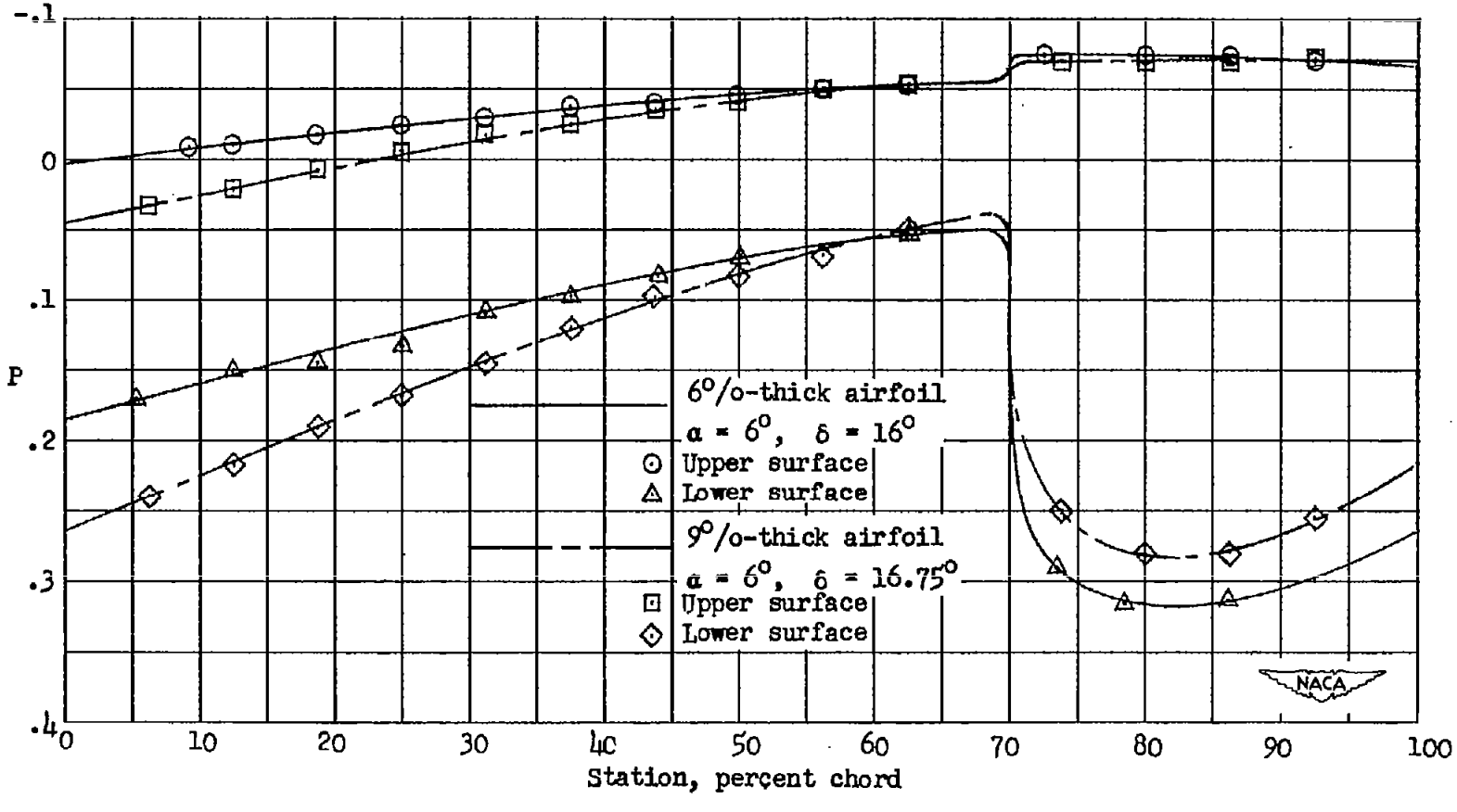

(c) $\alpha = 6^{\circ}$.

Figure 11.- Continued.

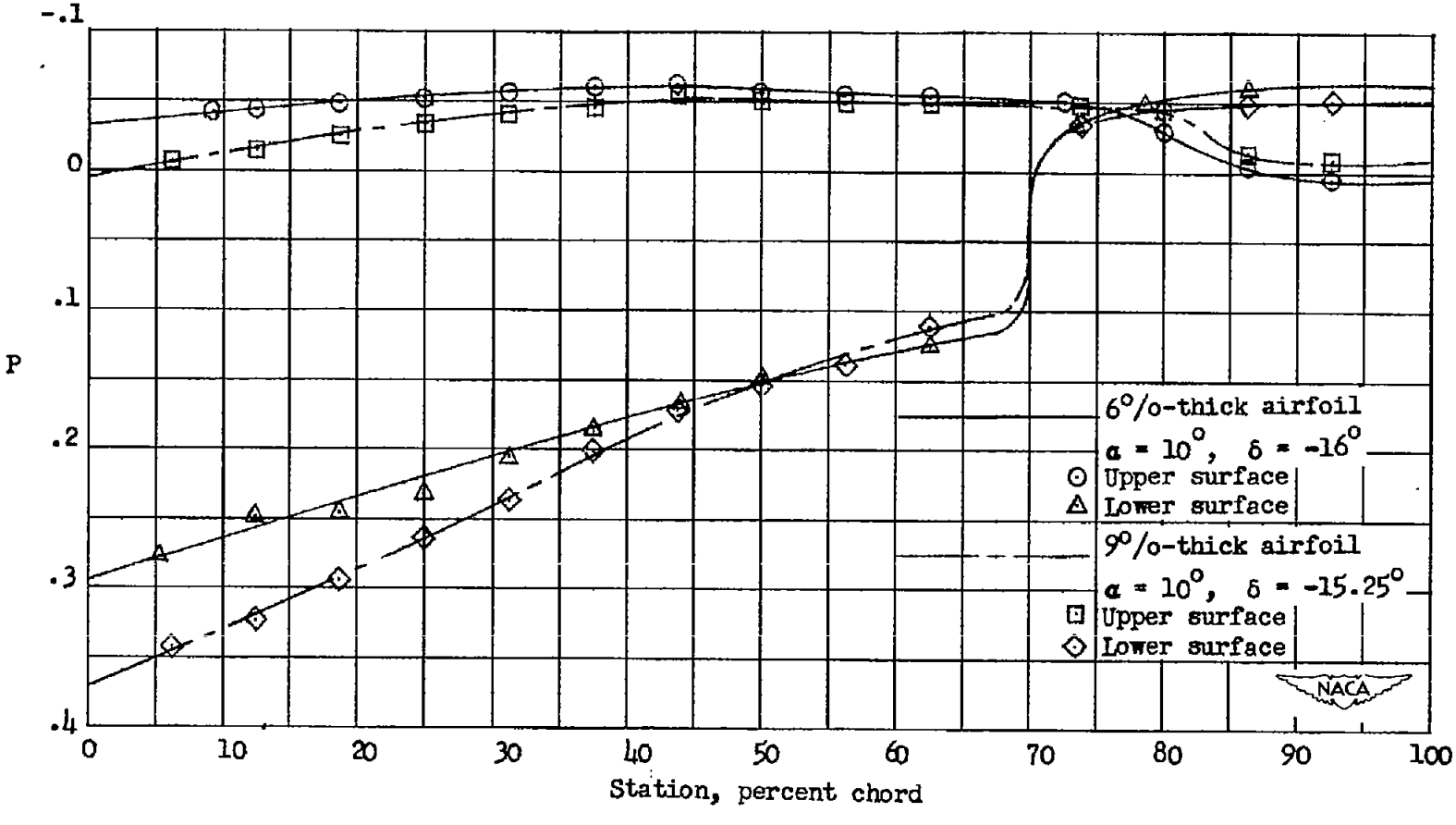

(d) $\alpha = 10^{\circ}$.

Figure 11.- Concluded.

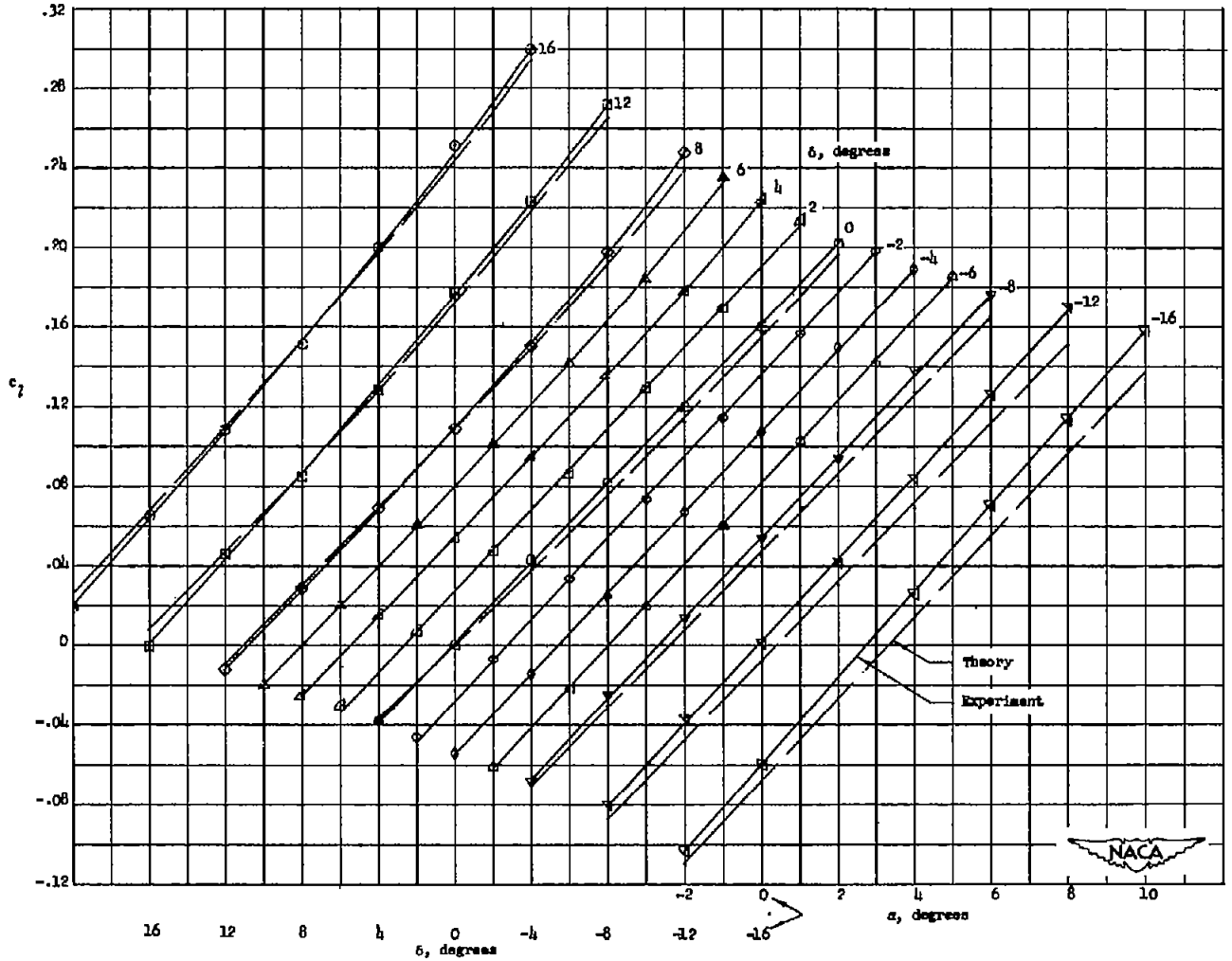

(a) 6-percent-thick airfoil.

Figure 12.- The variation of section lift coefficient with angle of attack and flap angle for 6- and 9-percent-thick symmetrical circular-arc airfoils with 30-percent-chord trailing-edge flaps. M, 4.04; R, 5×10^6.

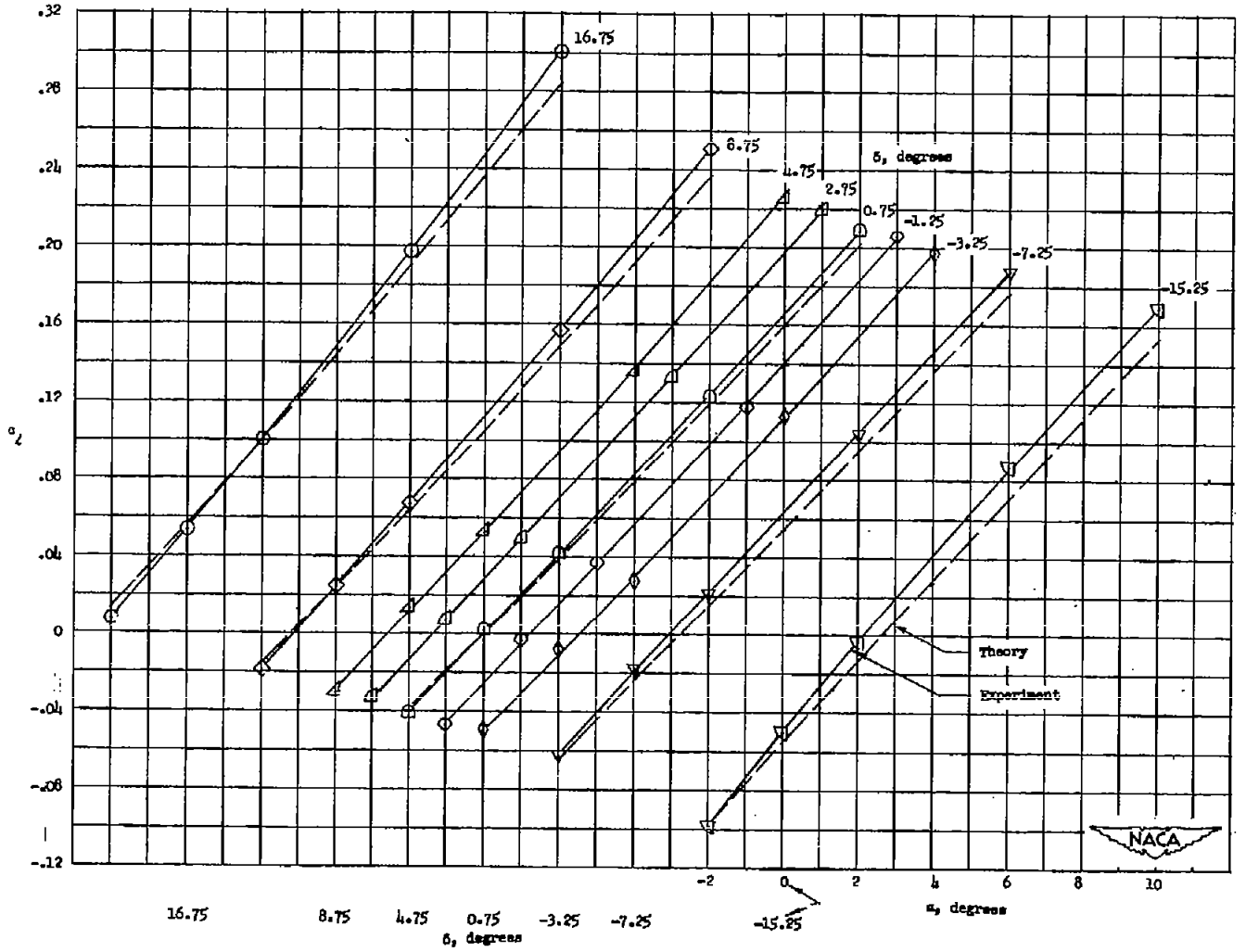

(b) 9-percent-thick airfoil.

Figure 12.- Continued.

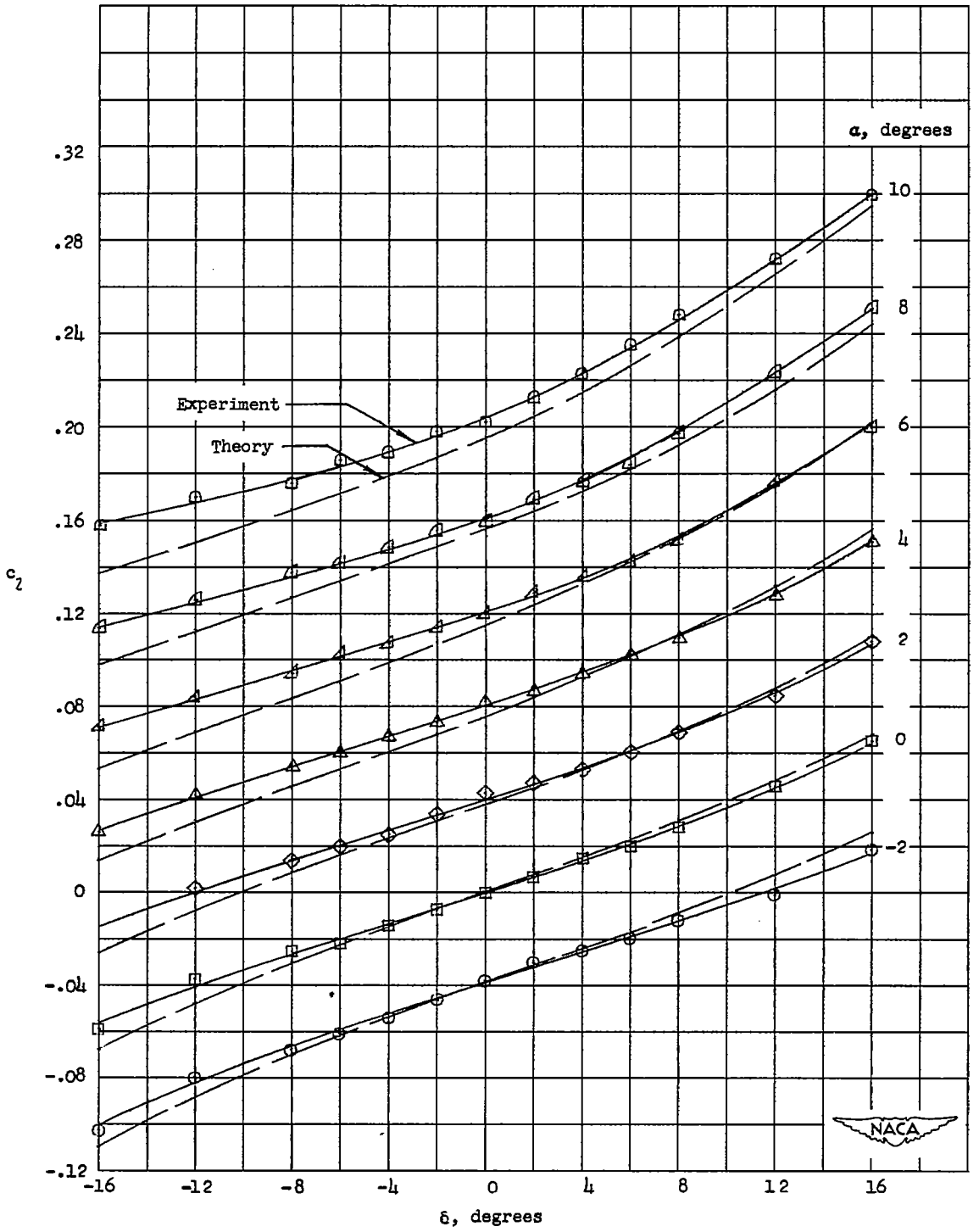

(c) 6-percent-thick airfoil.

Figure 12.- Continued.

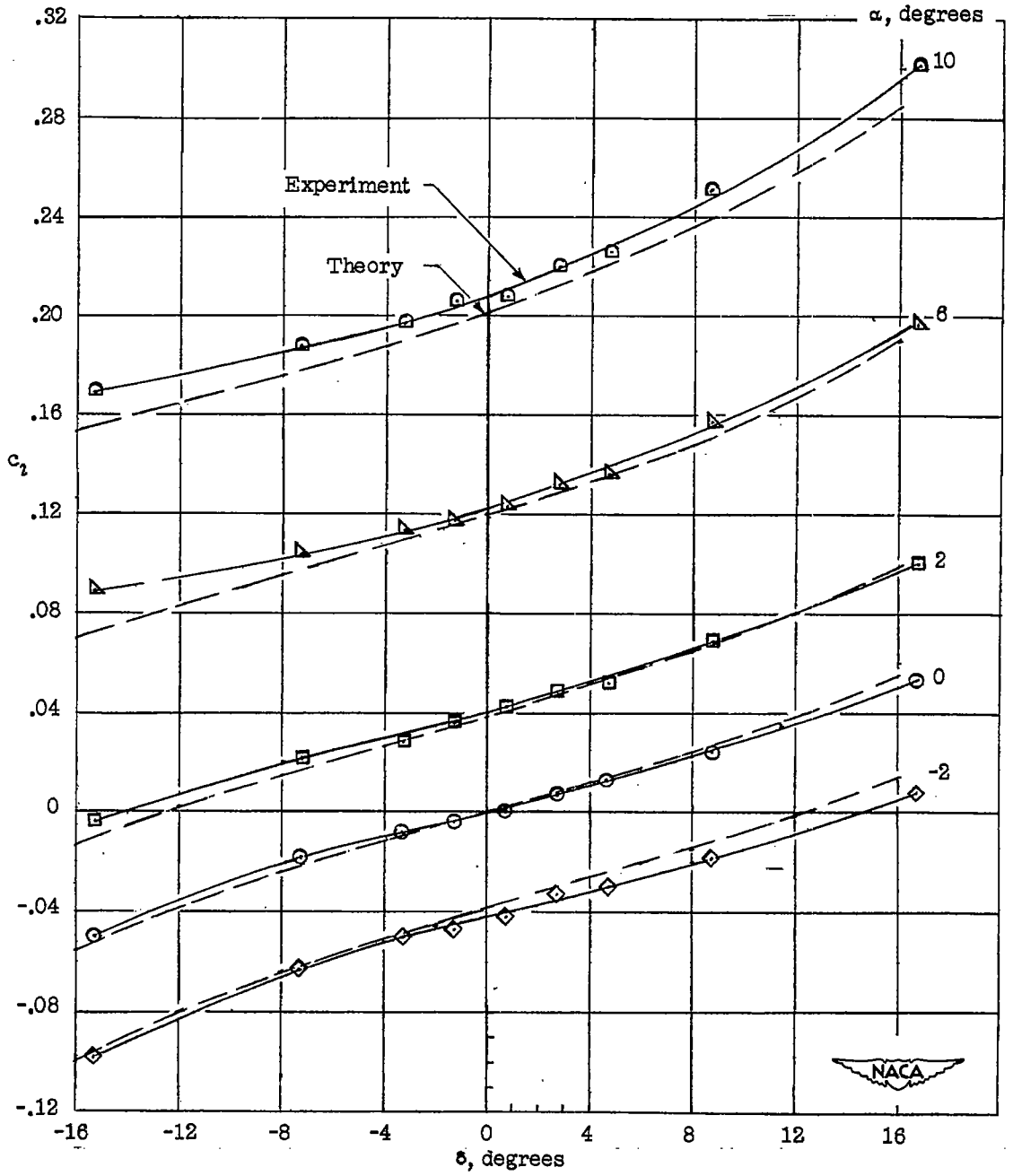

(d) 9-percent-thick airfoil.

Figure 12.- Concluded.

[redacted]

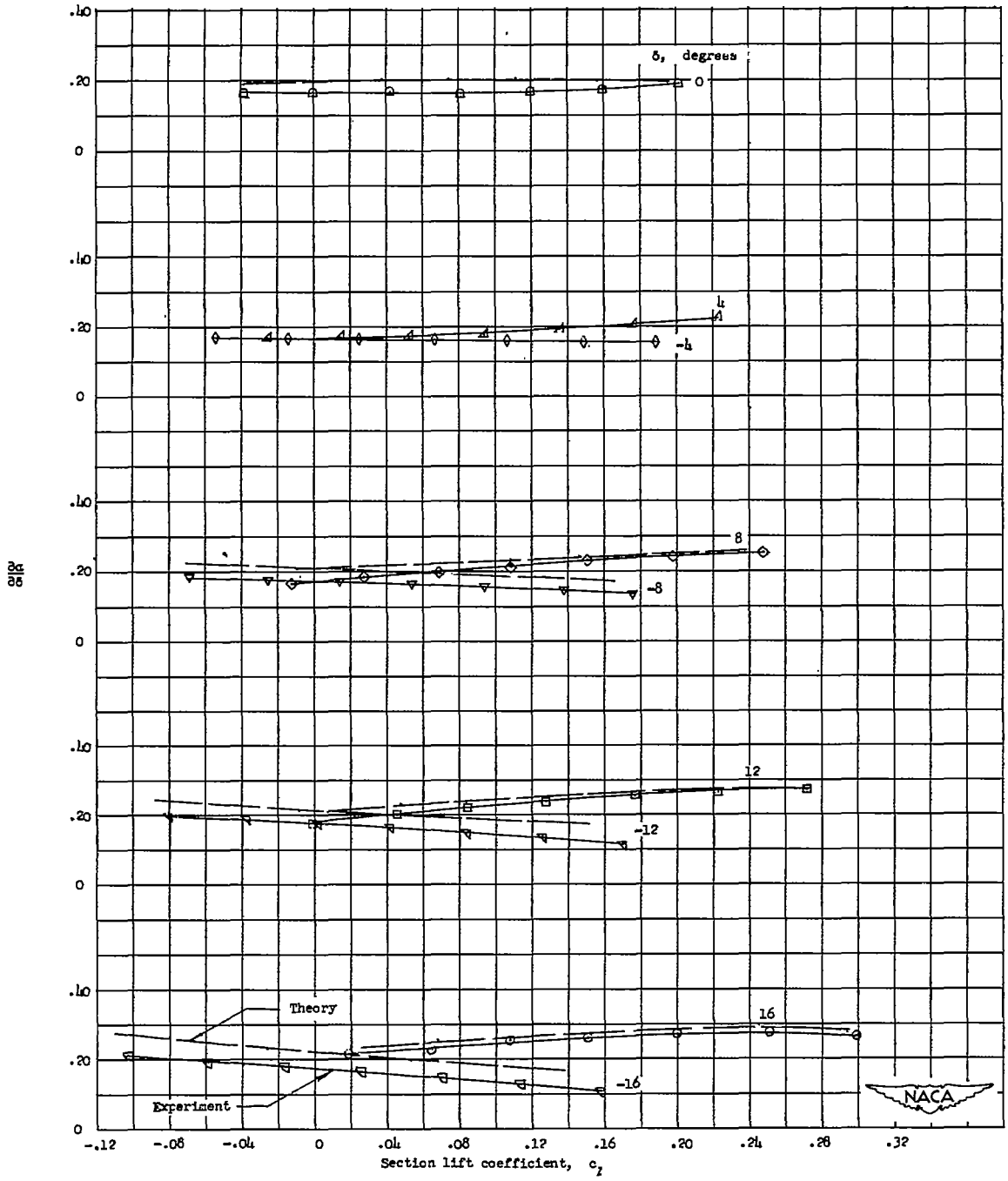

(a) 6-percent-thick airfoil.

Figure 13.- The variation of the flap effectiveness factor with section lift coefficient at several flap angles for 6- and 9-percent-thick symmetrical circular-arc airfoils with 30-percent-chord trailing-edge flaps. M, 4.04; R, 5×10^6.

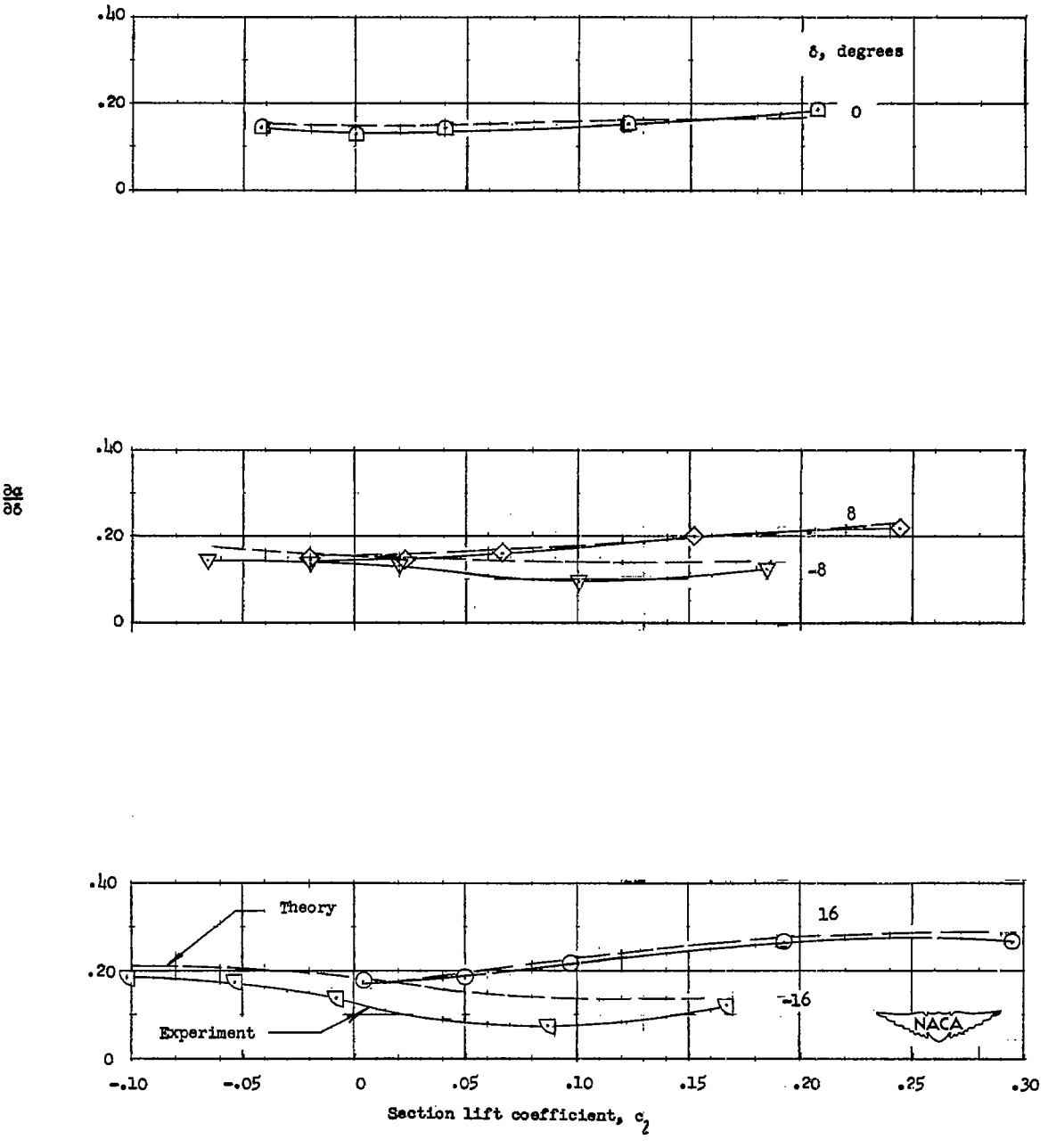

(b) 9-percent-thick airfoil.

Figure 13.- Concluded.

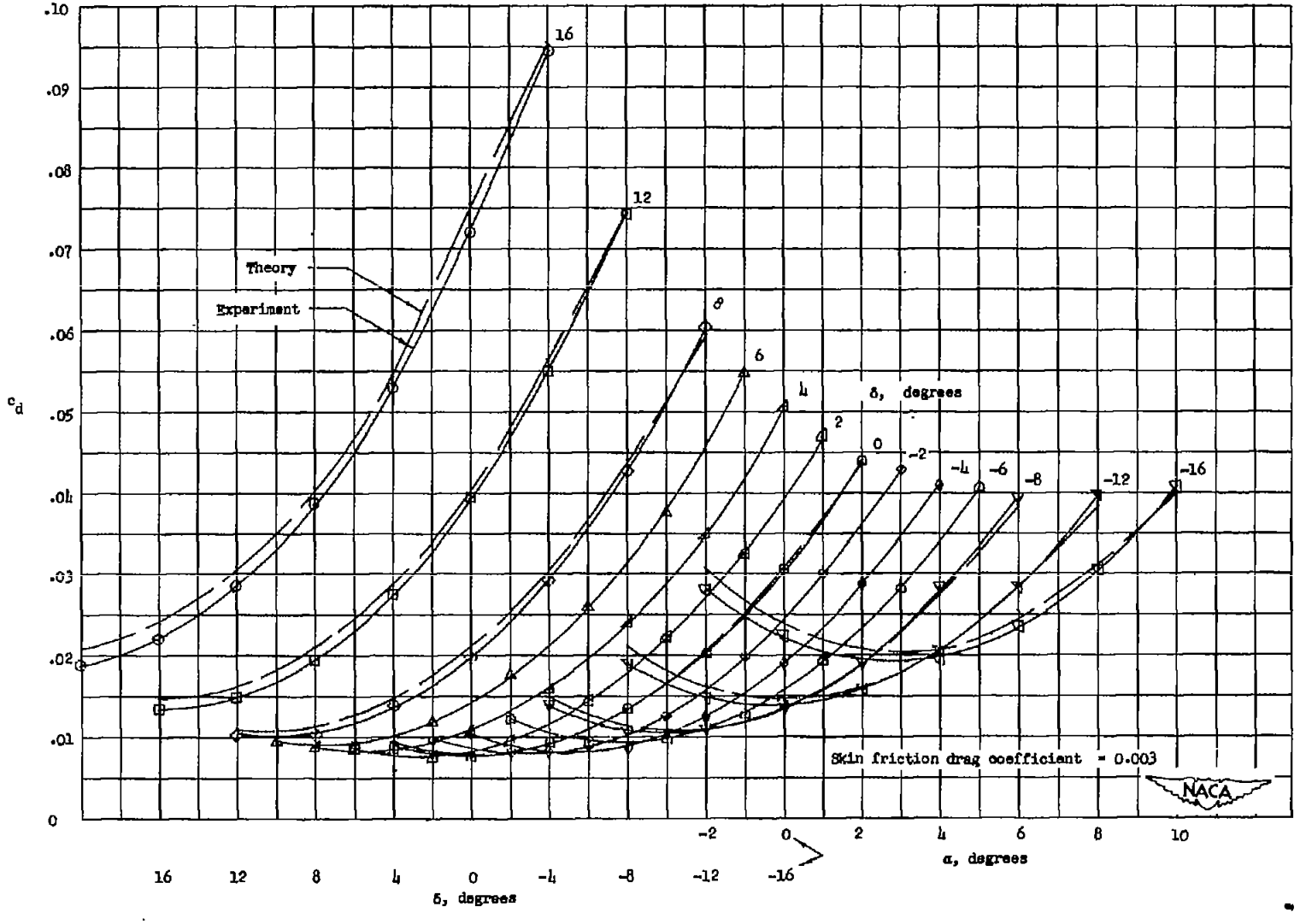

(a) 6-percent-thick airfoil.

Figure 14.- The variation of section drag coefficient with angle of attack and flap angle for 6- and 9-percent-thick symmetrical circular-arc airfoils with 30-percent-chord trailing-edge flaps. M, 4.04; R, 5×10^6.

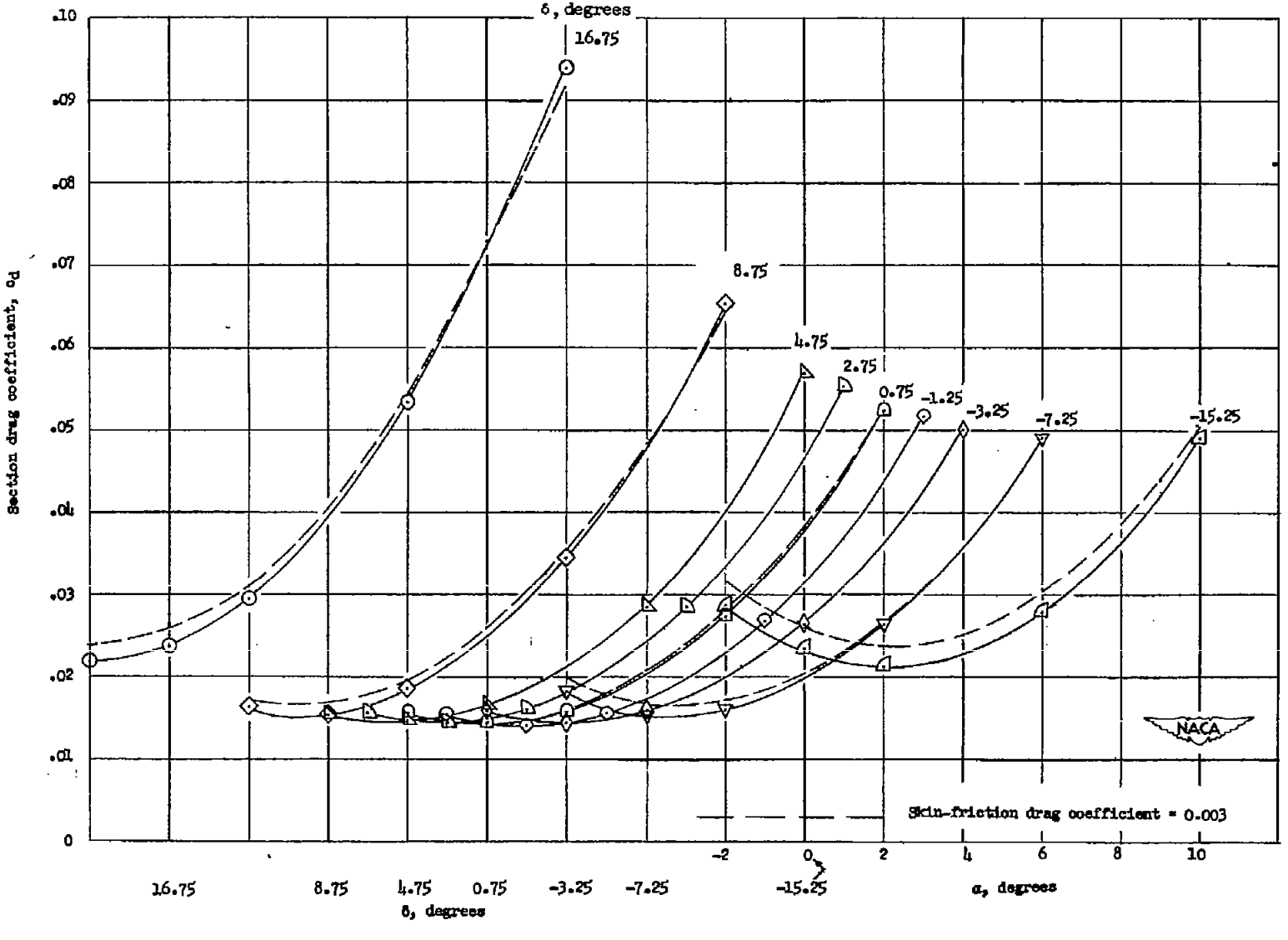

(b) 9-percent-thick airfoil.

Figure 14.- Concluded.

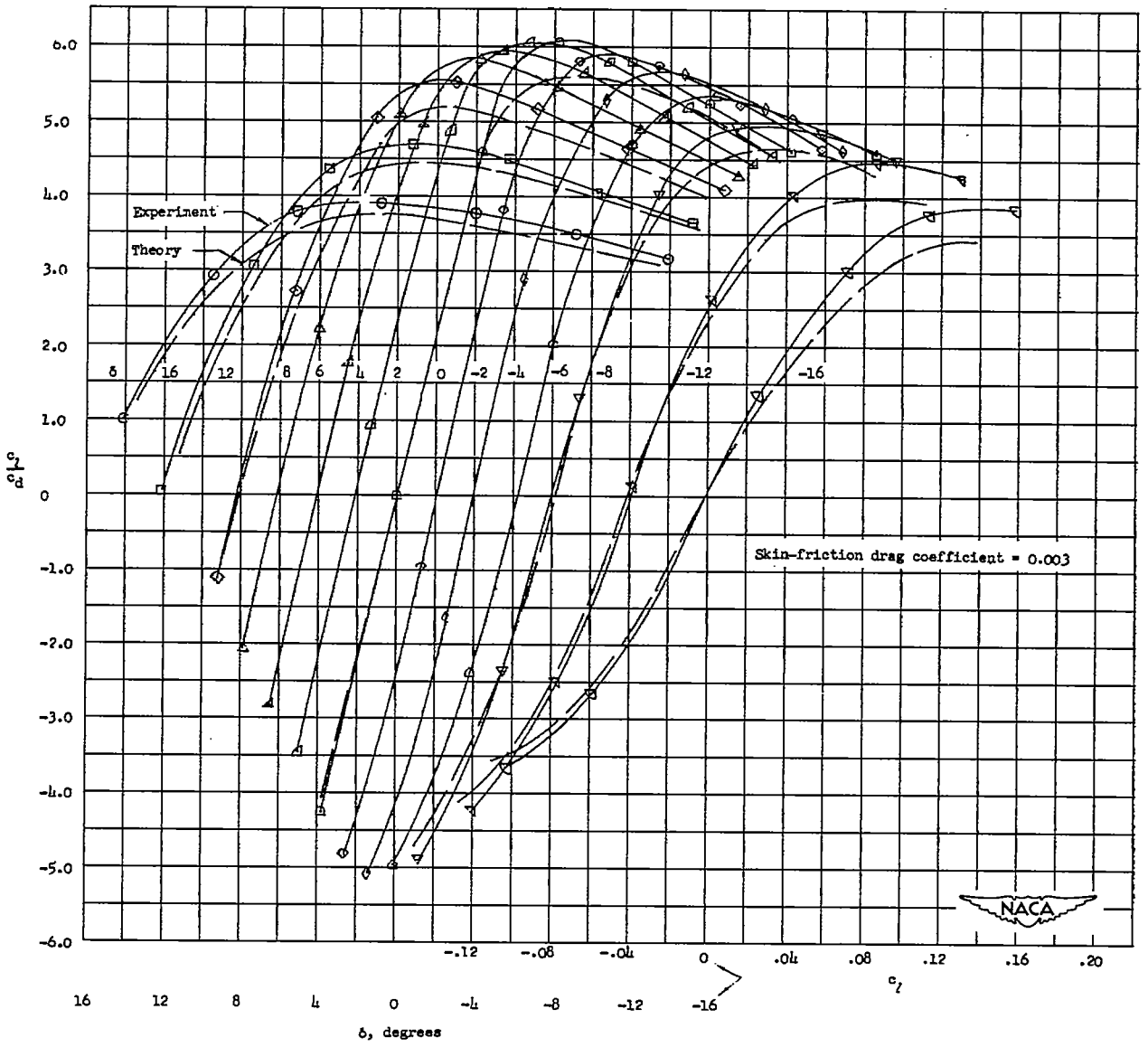

(a) 6-percent-thick airfoil.

Figure 15.- The variation of section lift-drag ratio with angle of attack and flap angle for 6- and 9-percent-thick symmetrical circular-arc airfoils with 30-percent-chord trailing-edge flaps. M, 4.04; R, 5×10^6.

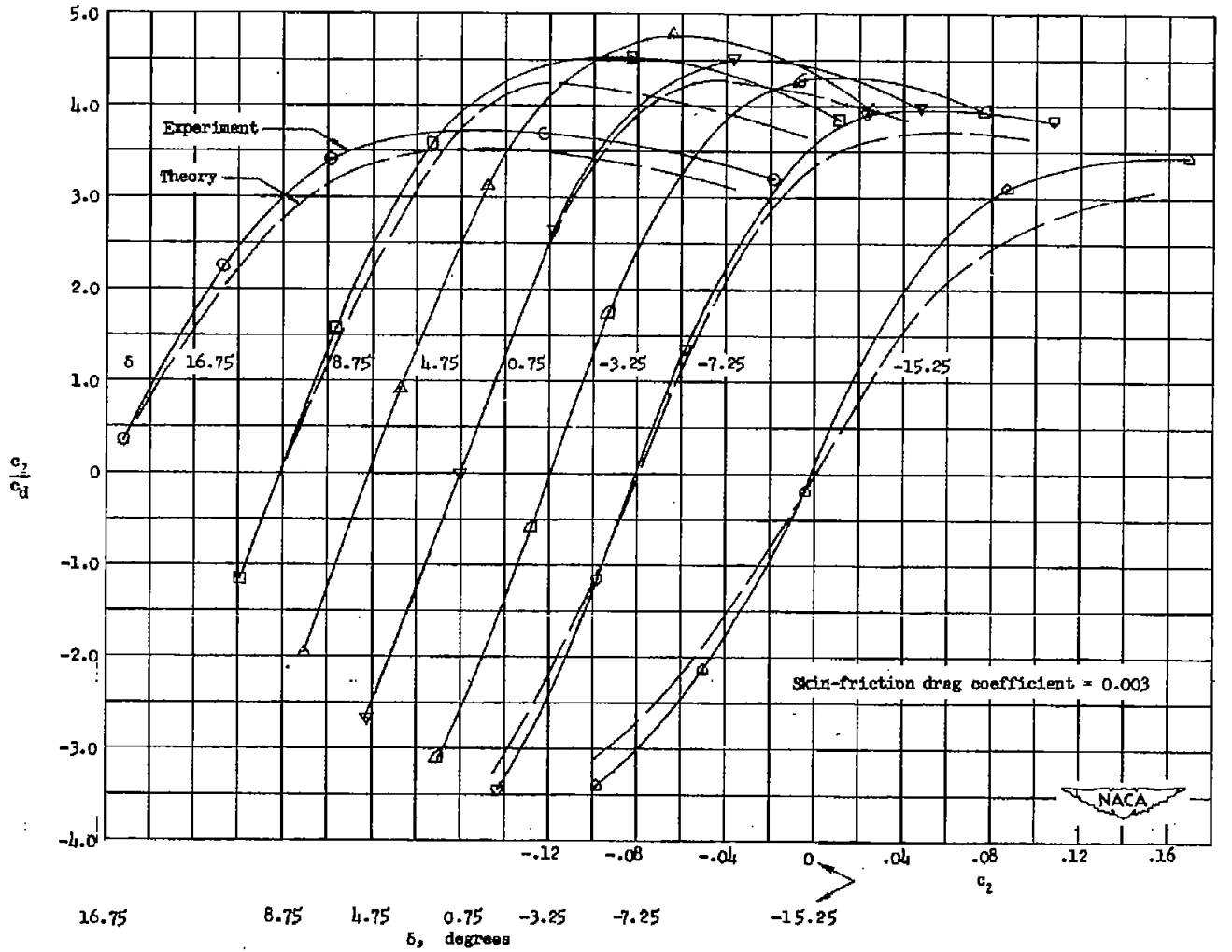

(b) 9-percent-thick airfoil.

Figure 15.- Concluded.

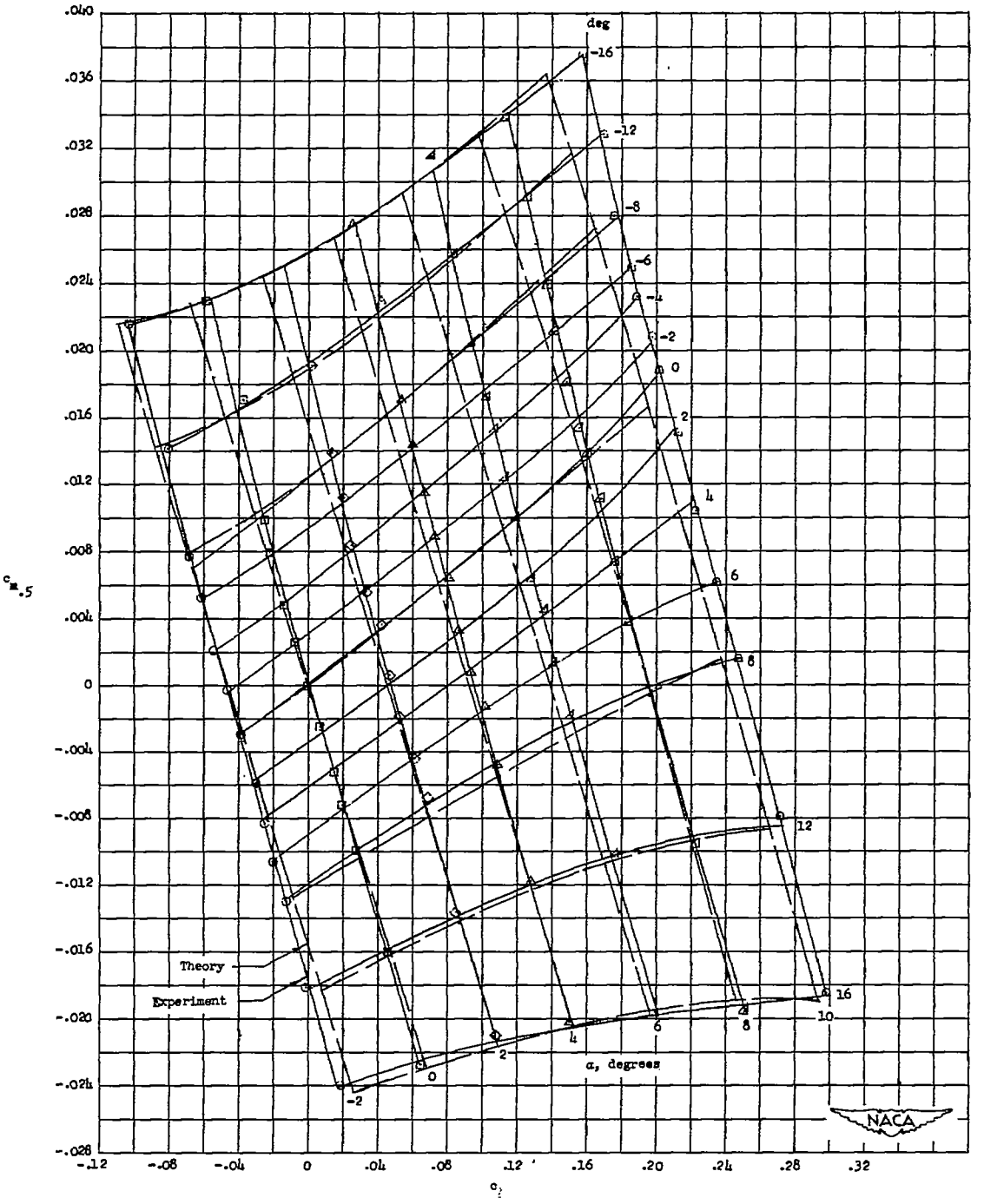

(a) 6-percent-thick airfoil.

Figure 16.- Variation of section pitching moment with section lift coefficient for constant angles of attack and flap angles for 6- and 9-percent-thick symmetrical circular-arc airfoils with 30-percent-chord trailing-edge flaps. M, 4.04; R, 5 × 10[redacted]6.

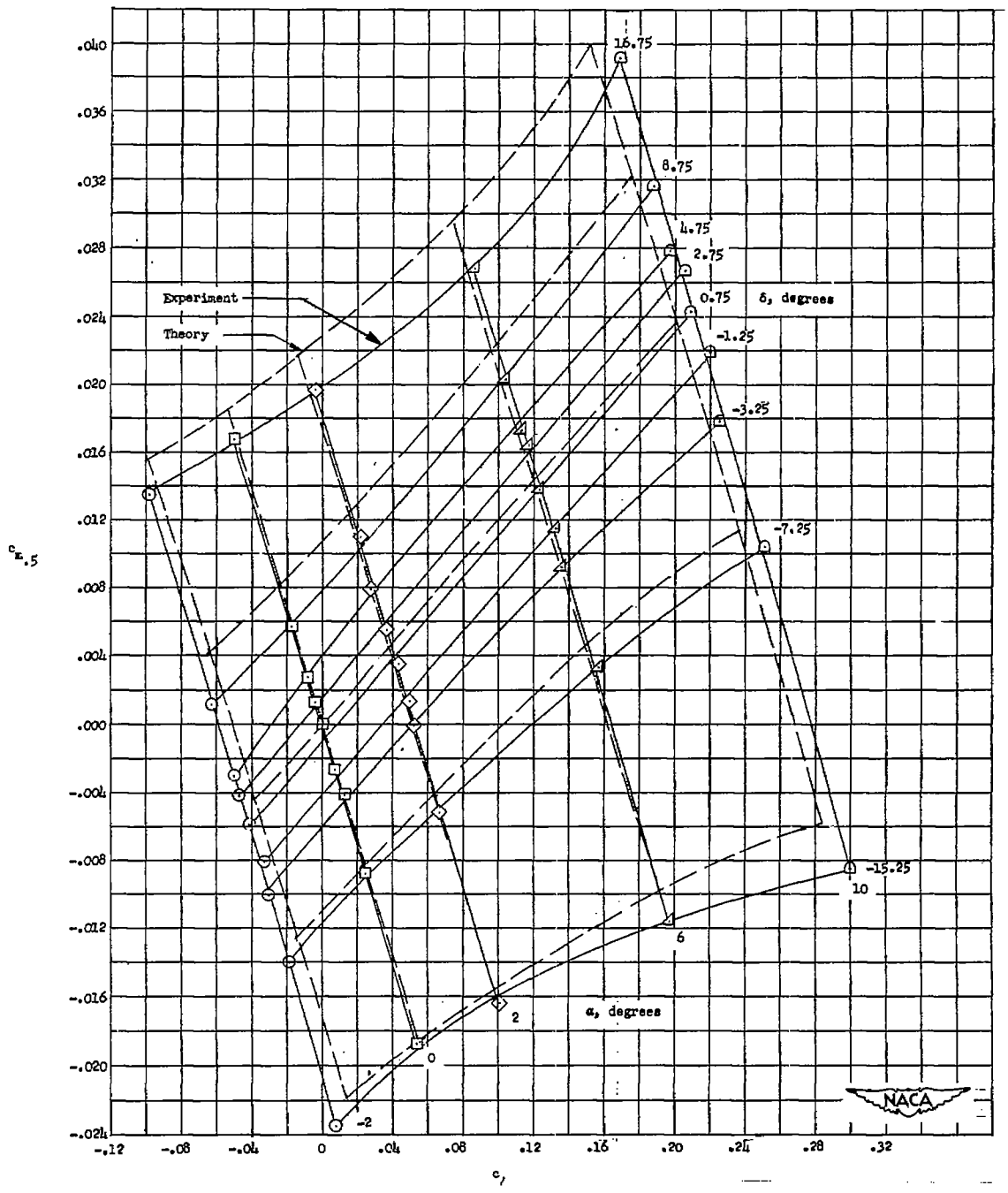

(b) 9-percent-thick airfoil.

Figure 16.- Concluded.

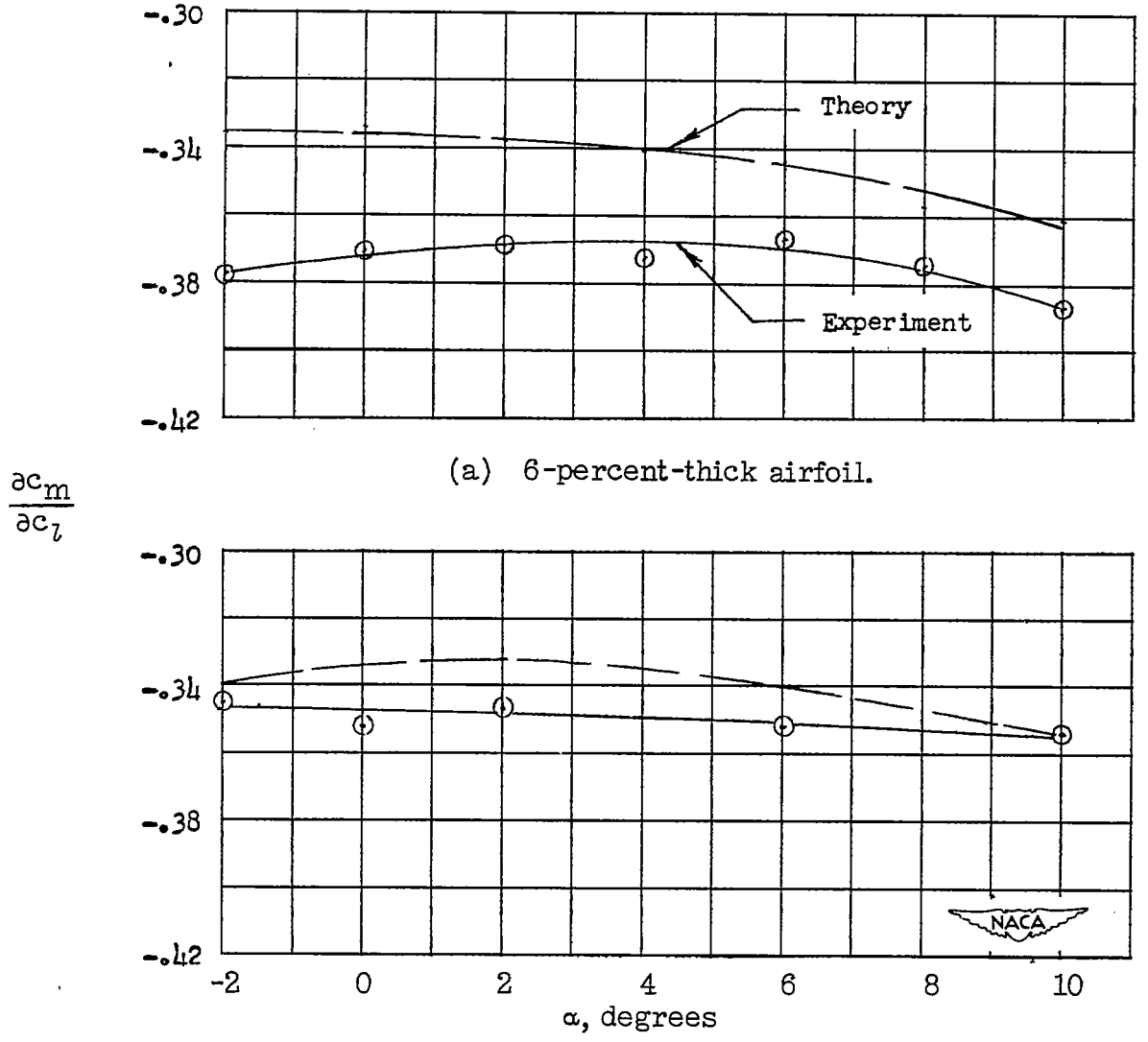

Figure 17.- The rate of change of section pitching-moment coefficient with section lift coefficient at zero pitching moment for constant angle of attack for 6- and 9-percent-thick symmetrical circular-arc airfoils with 30-percent-chord trailing-edge flaps. M, 4.04; R, 5×10^6.

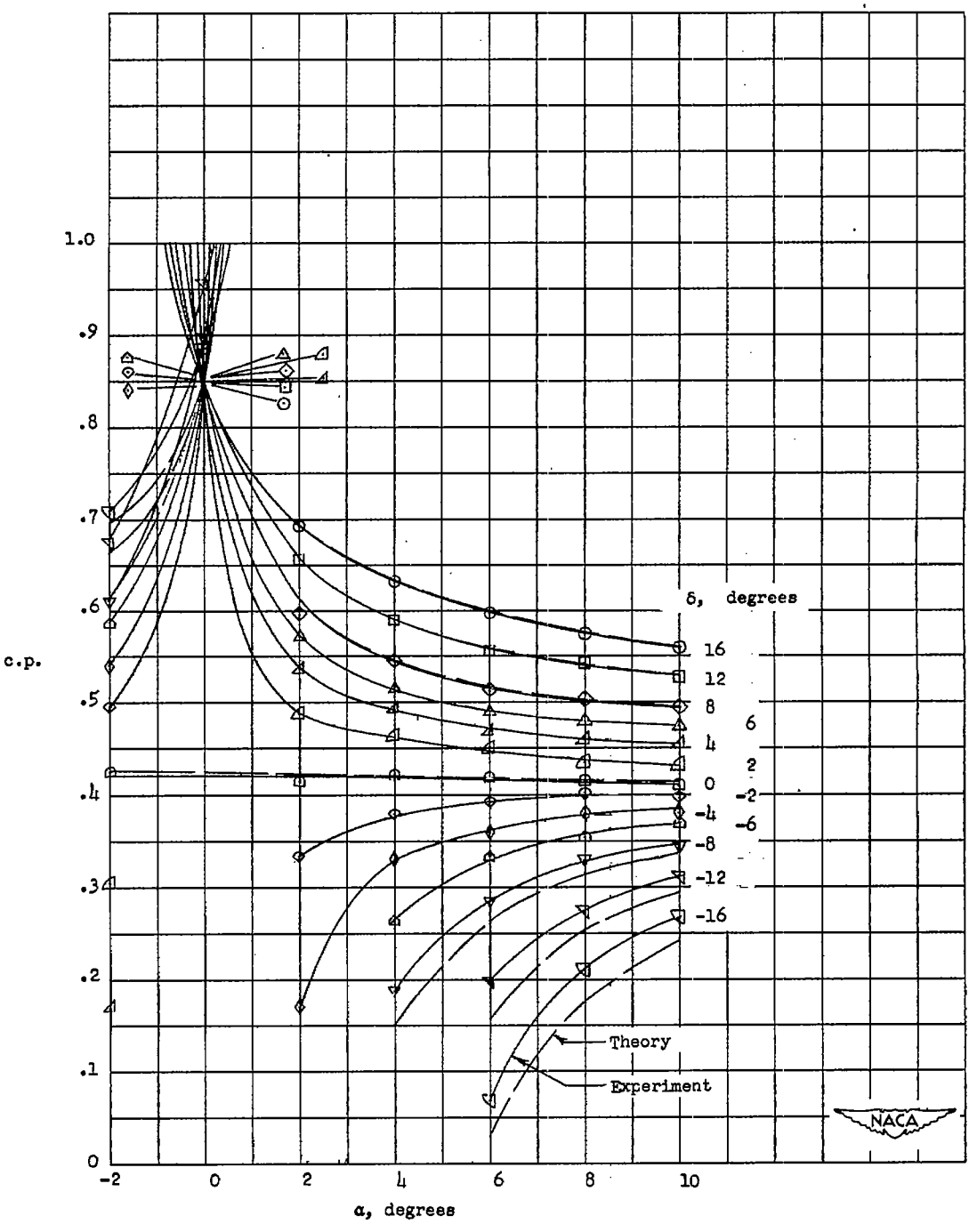

(a) 6-percent-thick airfoil.

Figure 18.- Movement of the center of pressure at several flap angles with angle of attack for 6- and 9-percent-thick symmetrical circular-arc airfoils with 30-percent-chord trailing-edge flaps. M, 4.04; R, 5×10^6.

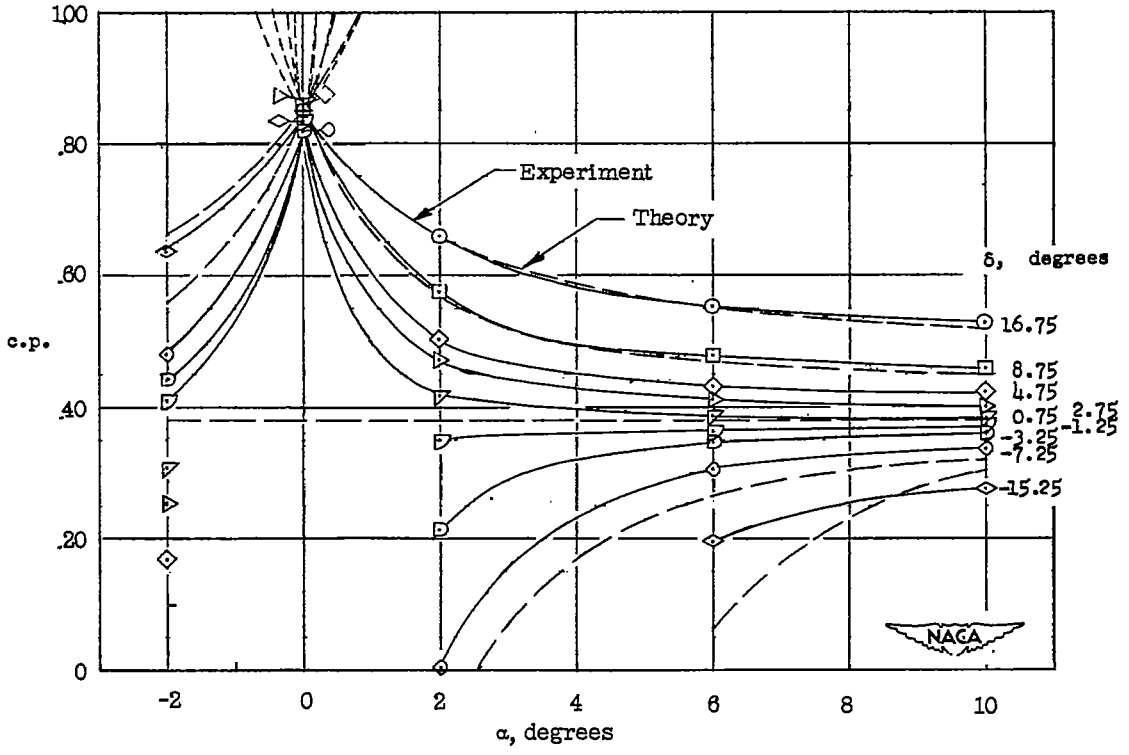

(b) 9-percent-thick airfoil.

Figure 18.- Concluded.

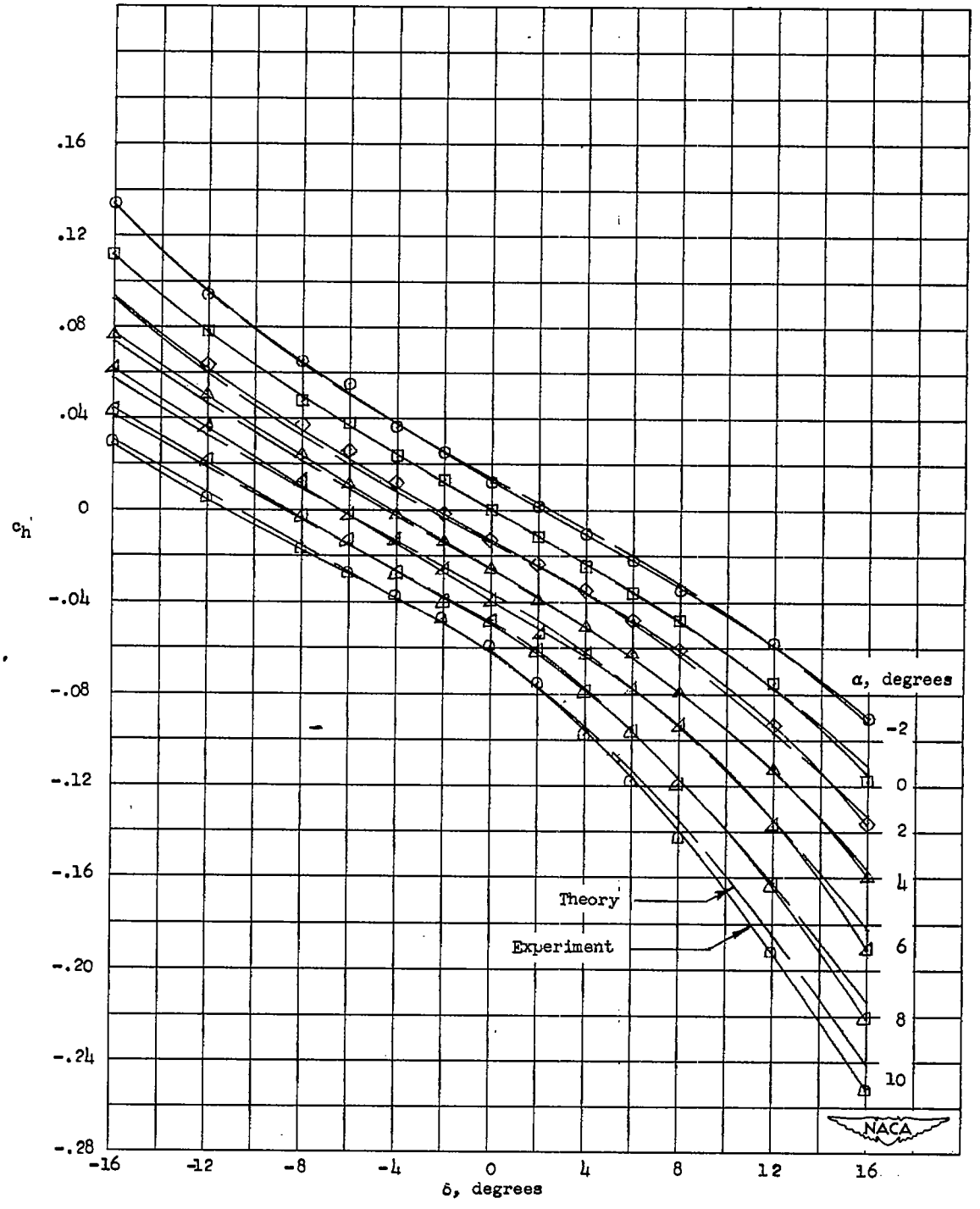

(a) 6-percent-thick airfoil.

Figure 19.- The variation of section hinge-moment coefficient with flap angle for 6- and 9-percent-thick symmetrical circular-arc airfoils with 30-percent-chord trailing-edge flaps. M, 4.04; R, 5×10^6.

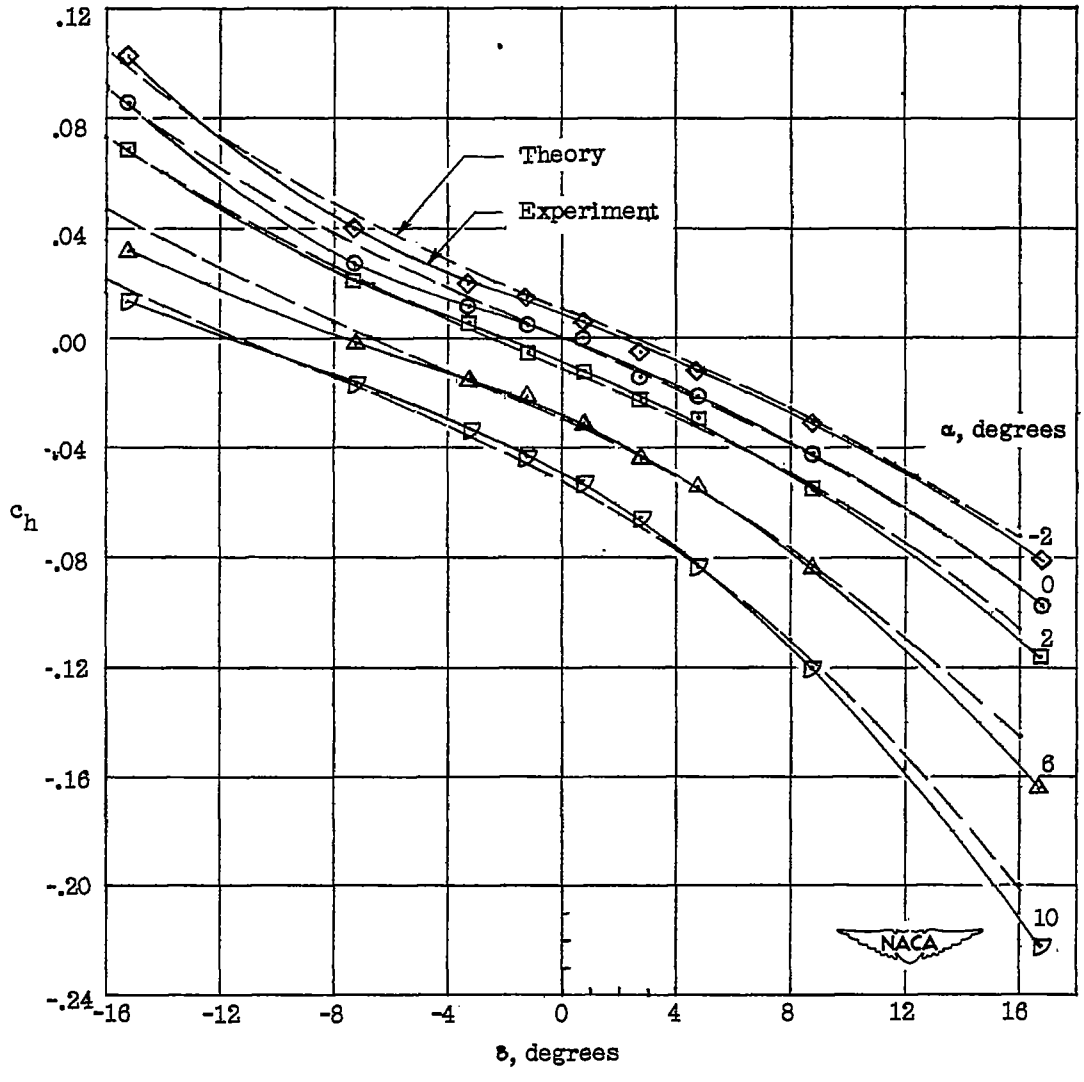

(b) 9-percent-thick airfoil.

Figure 19.- Concluded.

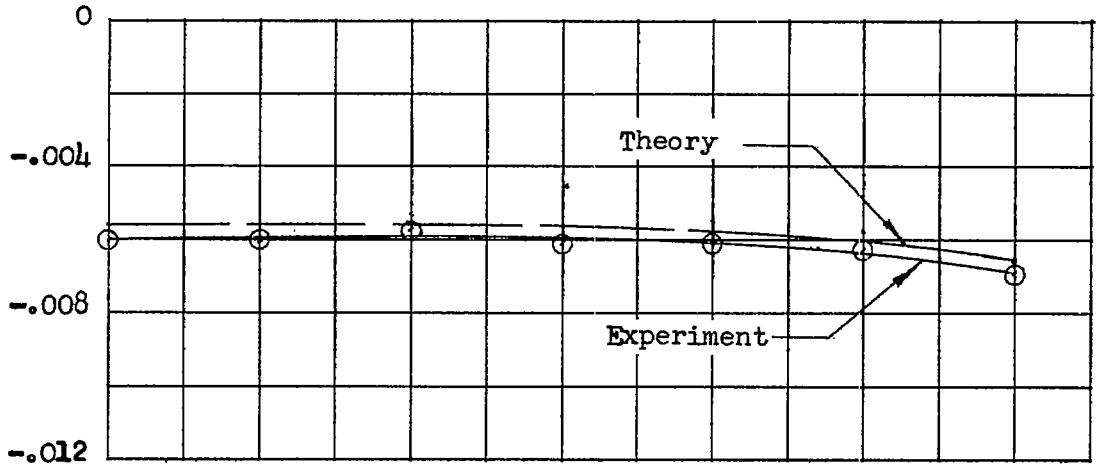

(a) 6-percent-thick airfoil.

c_{h_δ}

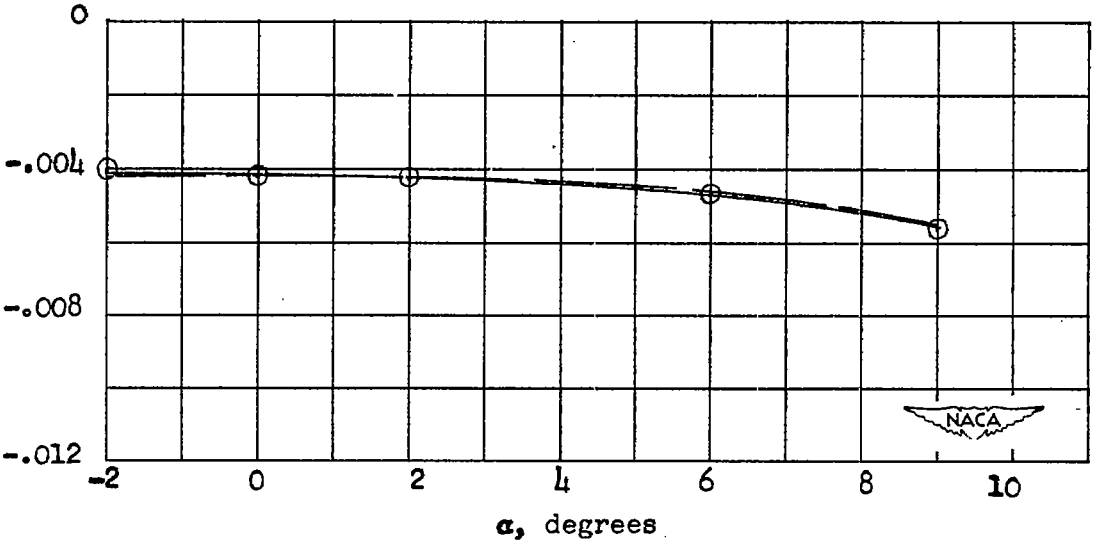

(b) 9-percent-thick airfoil.

Figure 20.- The variation of section hinge-moment slope parameter with angle of attack for 6- and 9-percent-thick symmetrical circular-arc airfoils with 30-percent-chord trailing-edge flaps. M, 4.04; R, 5×10^6.

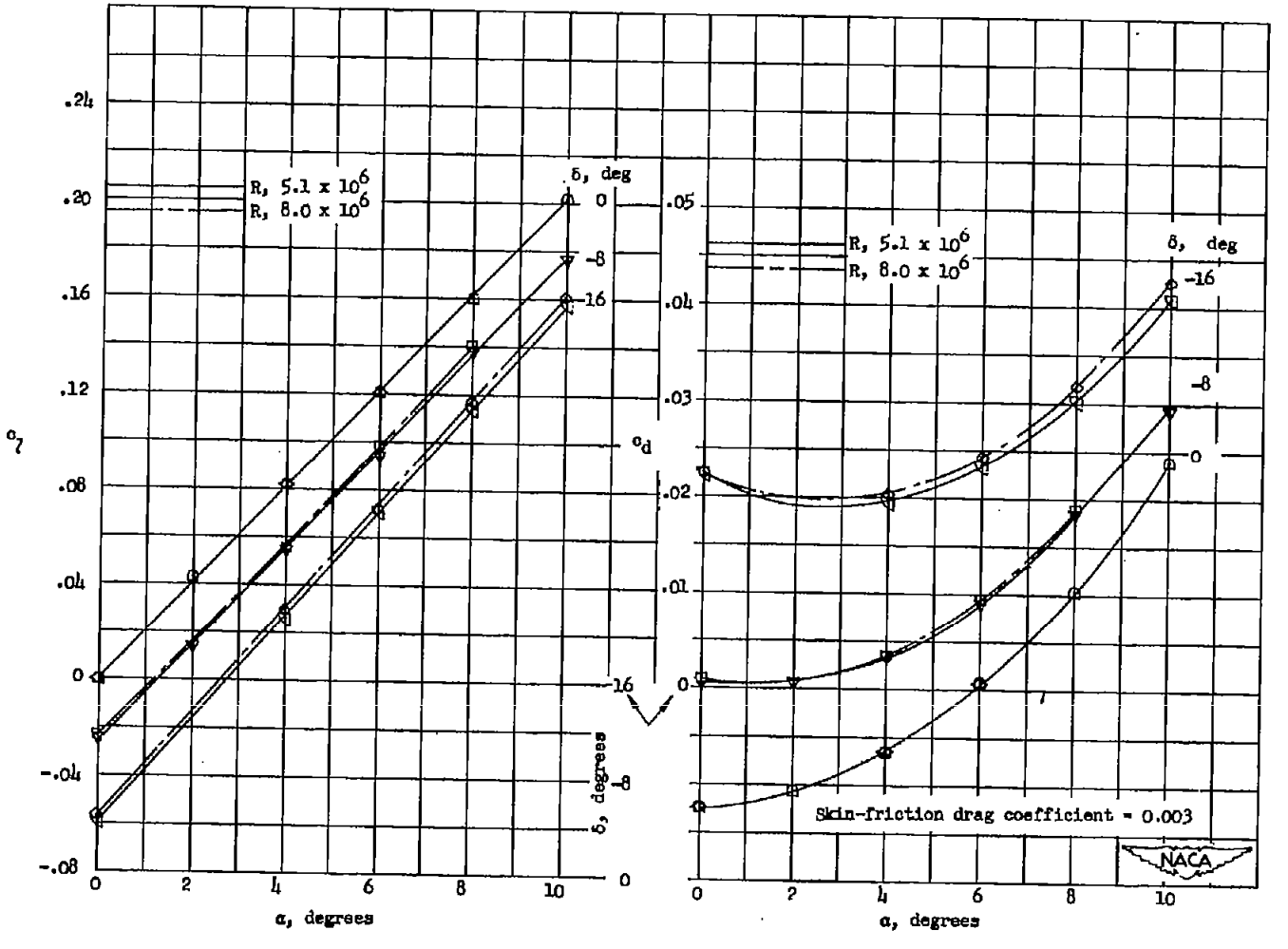

(a) Section lift coefficient. (b) Section drag coefficient.

Figure 21.- The effect of Reynolds number on the force and moment coefficients of the 6-percent-thick symmetrical circular-arc airfoil with 30-percent chord trailing-edge flap. M, 4.04.

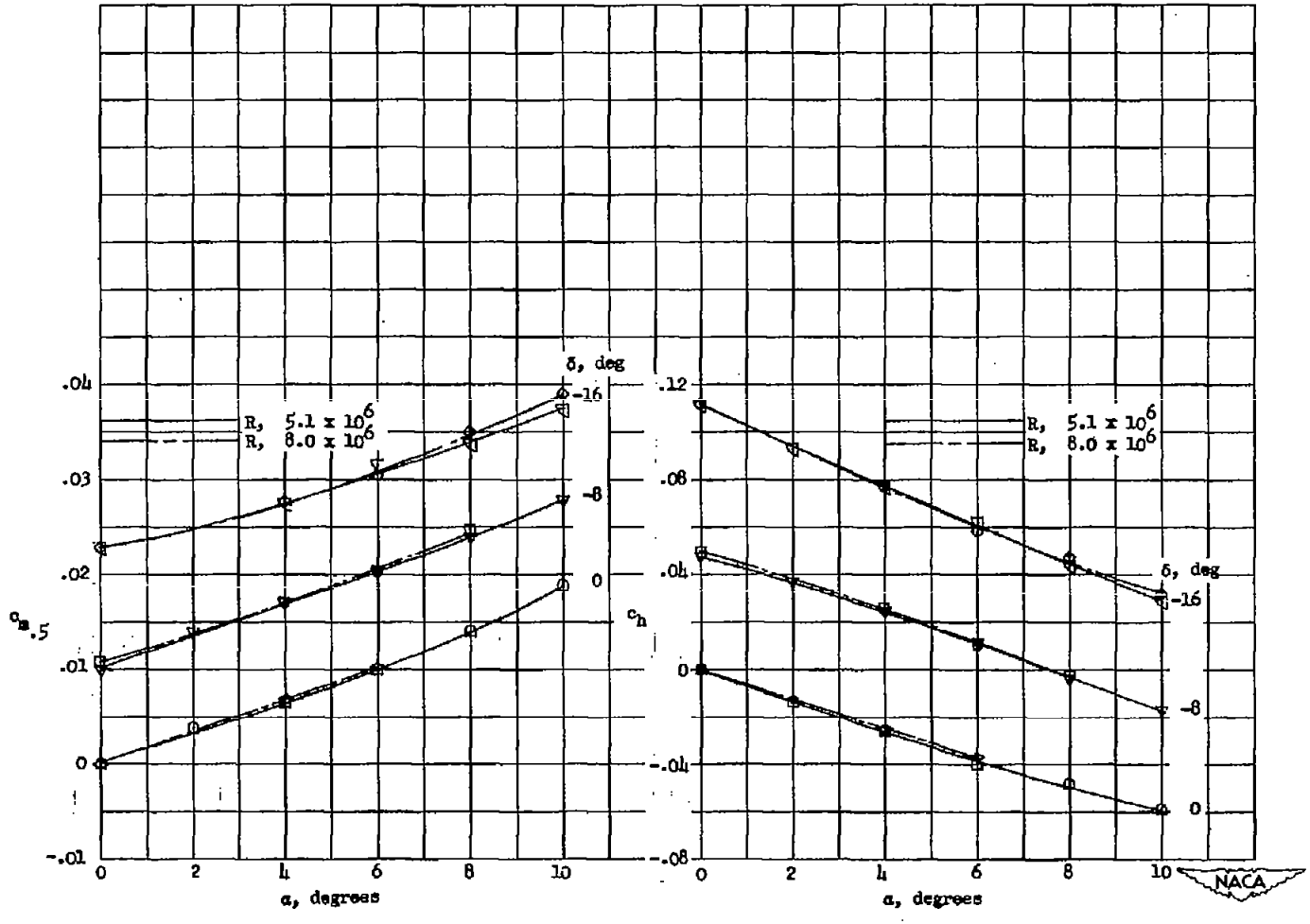

(c) Section pitching-moment coefficient. (d) Section hinge-moment coefficient.

Figure 21.- Concluded.

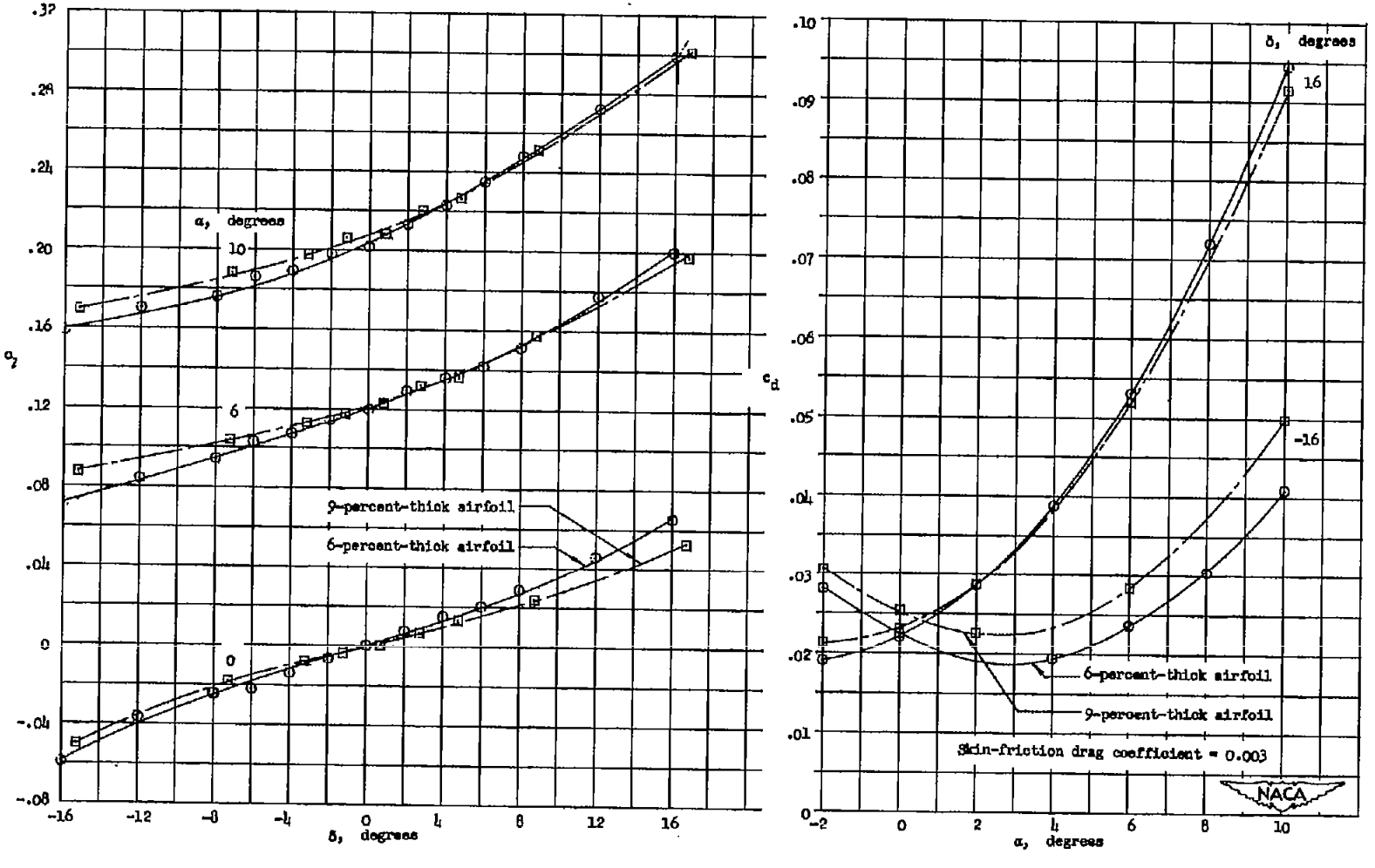

(a) Section lift coefficient. (b) Section drag coefficient.

Figure 22.- The effect of changing airfoil thickness on the force and moment coefficients of symmetrical circular-arc airfoils with 30-percent-chord trailing-edge flaps. M, 4.04; R, 5×10^6.

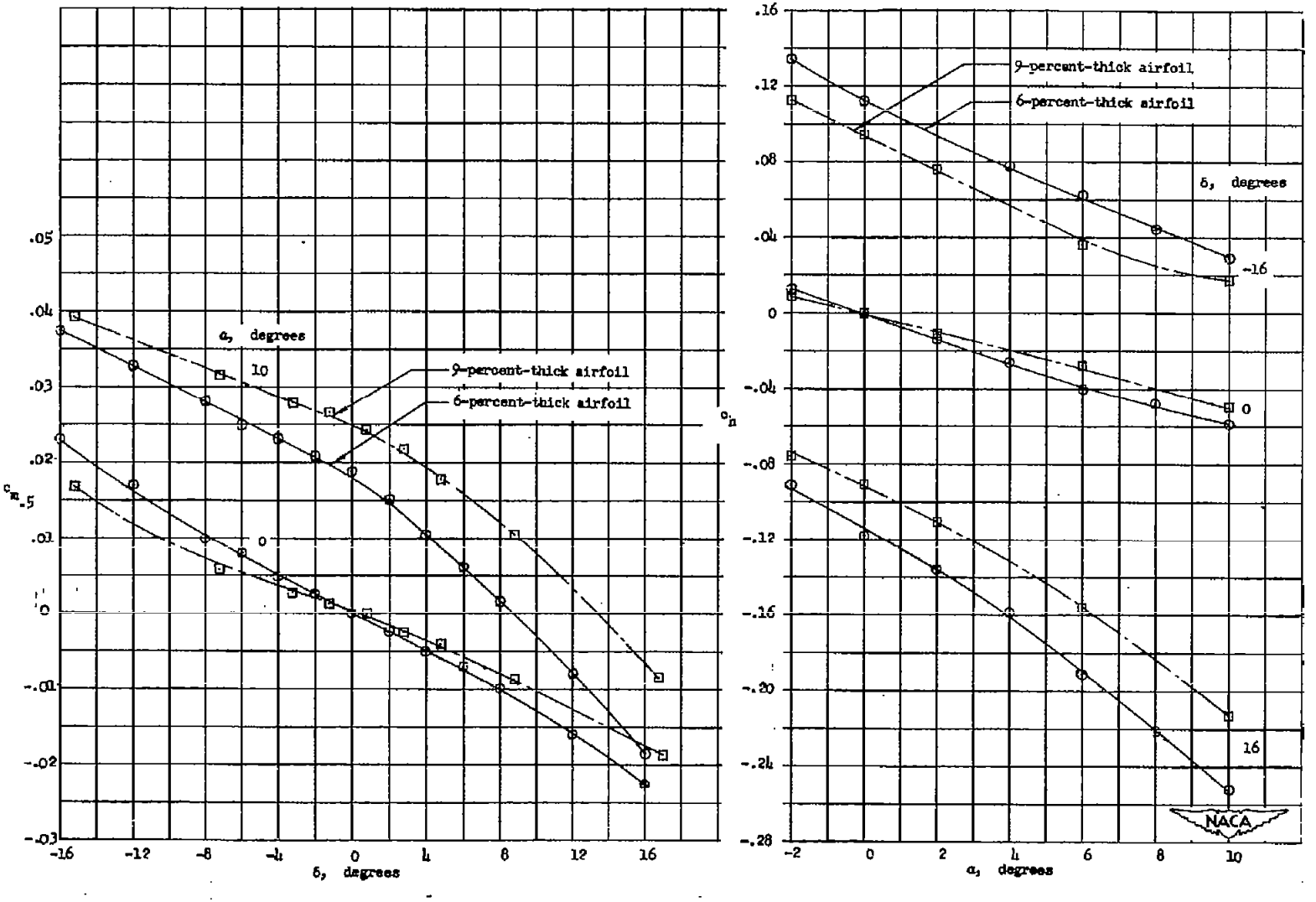

(c) Section pitching-moment coefficient. (d) Section hinge-moment coefficient.

Figure 22.- Concluded.

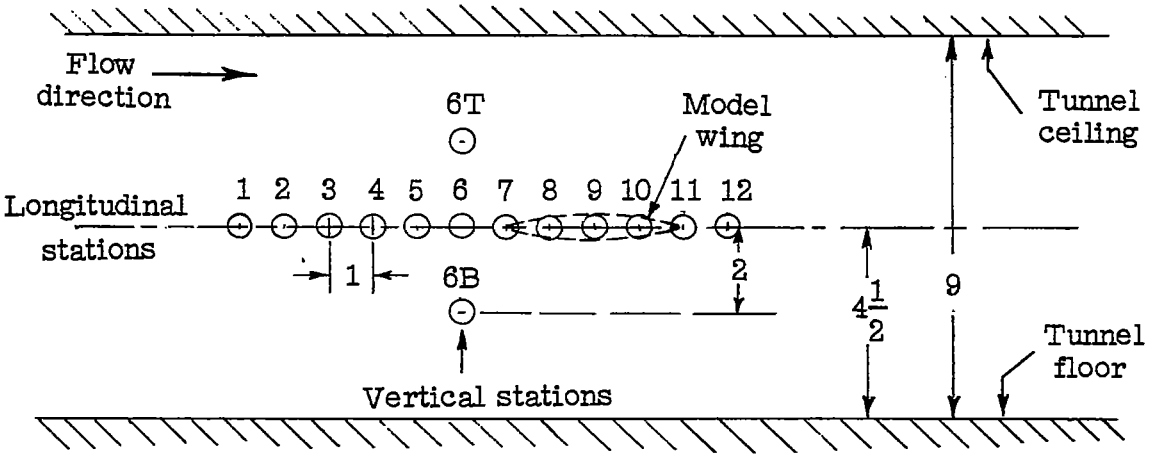

(a) Side view of the test section showing the location of longitudinal and vertical survey stations.

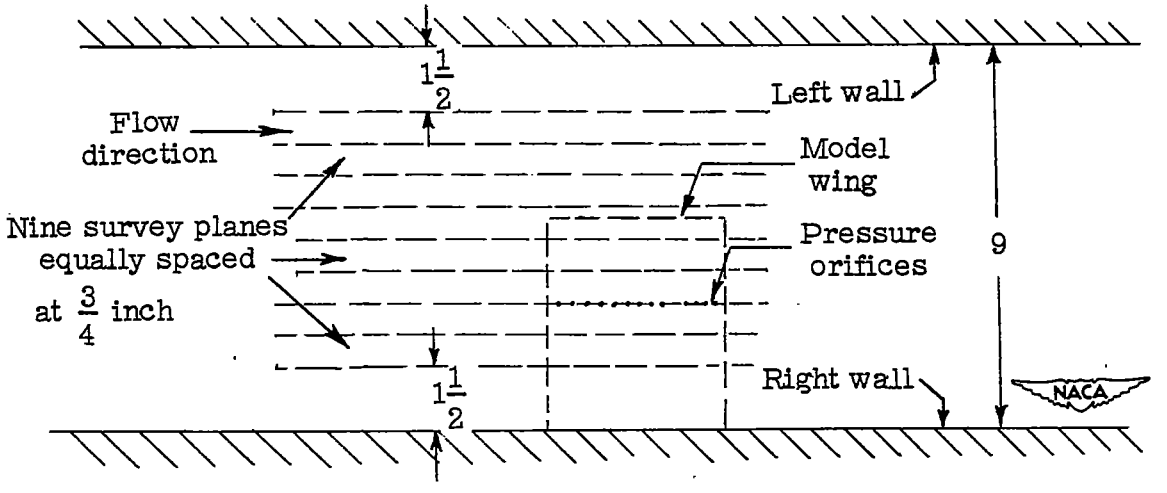

(b) Plan view of the test section showing the lateral location of the planes in which the longitudinal and vertical surveys were obtained.

Figure 23.- Side view and plan view of the test section of the Langley 9- by 9-inch Mach number 4 blowdown tunnel showing the position of the survey stations.

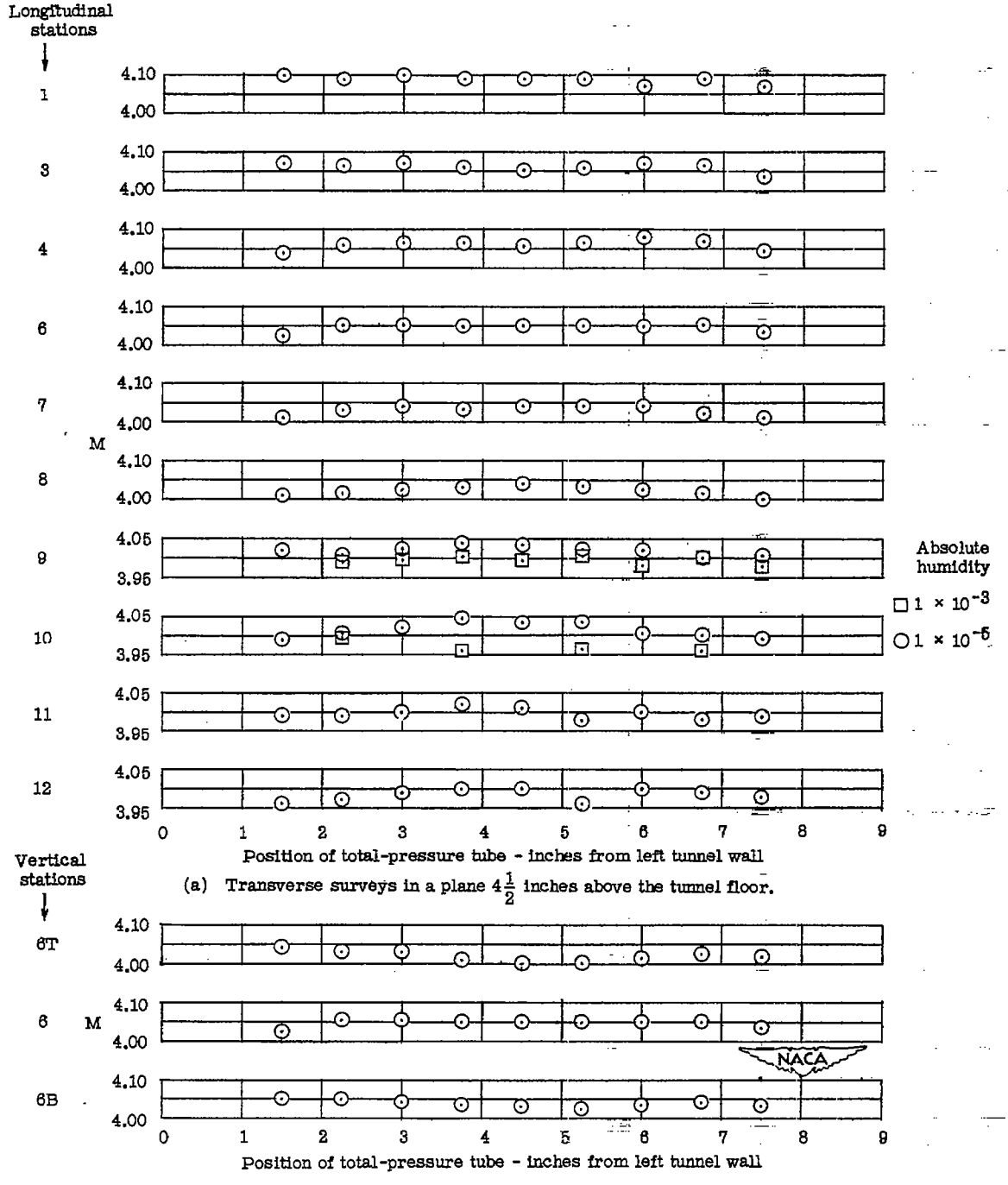

(a) Transverse surveys in a plane $4\frac{1}{2}$ inches above the tunnel floor.

(b) Transverse surveys in a vertical plane at longitudinal station no. 6.

Figure 24.- Mach numbers in the test section of the Langley 9- by 9-inch Mach number 4 blowdown tunnel as determined by total-pressure surveys.

NACA-Langley - 7-19-51 - 400

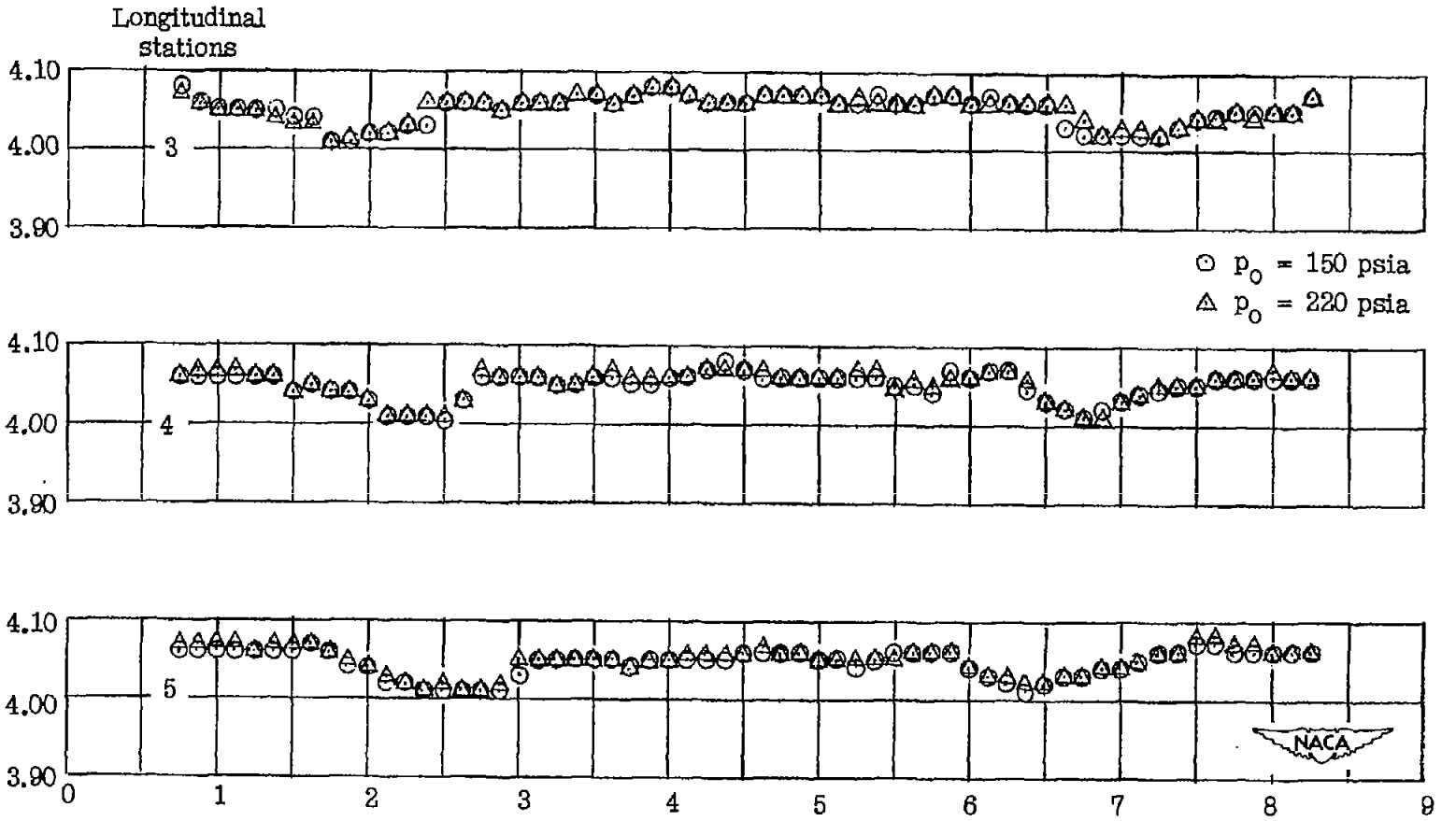

(c) Vertical surveys on tunnel center line at longitudinal stations -1, 0, and 1.

Figure 24.- Concluded.